

# Nonminimal Couplings and the Forgotten Field of Axion Inflation

Evan McDonough,<sup>1,2</sup> Alan H. Guth,<sup>1</sup> and David I. Kaiser<sup>1</sup>

<sup>1</sup>*Center for Theoretical Physics, Laboratory for Nuclear Science, and Department of Physics,  
Massachusetts Institute of Technology, Cambridge, MA 02139, USA*

<sup>2</sup>*Kavli Institute for Cosmological Physics and Enrico Fermi Institute,  
The University of Chicago, Chicago, IL 60637, USA*

(Dated: October 8, 2020)

We study the multifield dynamics of axion models nonminimally coupled to gravity. As usual, we consider a canonical  $U(1)$  symmetry-breaking model in which the axion is the phase of a complex scalar field. If the complex scalar field has a nonminimal coupling to gravity, then the (oft-forgotten) radial component can drive a phase of inflation prior to an inflationary phase driven by the axion field. In this setup, the mass of the axion field is dependent on the radial field because of the nonminimal coupling, and the axion remains extremely light during the phase of radial inflation. As the radial field approaches the minimum of its potential, there is a transition to natural inflation in the angular direction. In the language of multifield inflation, this system exhibits ultra-light isocurvature perturbations, which are converted to adiabatic perturbations at a fast turn, namely the onset of axion inflation. For models wherein the CMB pivot scale exited the horizon during radial inflation, this acts to suppresses the tensor-to-scalar ratio  $r$ , without generating CMB non-Gaussianity or observable isocurvature perturbations. Finally, we note that the interaction strength between axion and gauge fields is suppressed during the radial phase relative to its value during the axion-inflation phase by several orders of magnitude. This decouples the constraints on the inflationary production of gauge fields (e.g., from primordial black holes) from the constraints on their production during (p)reheating.

## I. INTRODUCTION

The axion field was proposed as a solution to the strong CP problem of the Standard Model of particle physics [1–3]. More recently, axions rose to prominence in early universe cosmology both as a candidate for the inflaton field [4–6] and as a candidate for cold dark matter [7–9], bolstered by interesting phenomenology of the characteristic axion coupling to gauge fields (e.g., Ref. [10]). These developments coincided with the discovery of flux compactifications of string theory, which generically include hundreds of axion fields [11–13].

As the Goldstone boson of a spontaneously broken (approximate) global  $U(1)$  symmetry, the axion is naturally described as the phase of a complex scalar field. Inherent in this construction is a second scalar field, the radial component, which plays the role of the order-parameter of the symmetry breaking. Thus, axion models, both as they were initially conceived [1–3], and in their modern incarnations, are inherently multifield theories. As such, the dynamics of such models during the early universe should be studied using techniques developed in recent years for the analysis of multifield inflation, with a focus on characteristically multifield phenomena such as isocurvature perturbations, primordial non-Gaussianity, and their compatibility with recent observations. (For reviews, see Refs. [14–16].)

Beginning nearly a decade prior to the proposal of the axion, physicists began to clarify that self-interacting scalar fields in curved spacetime will generically develop nonminimal couplings to gravity [17–25]. Even if the dimensionless nonminimal coupling constants  $\xi$  vanish at tree-level in a given model, they will be generated

by loop corrections, and hence they are required for self-consistent renormalization of scalar-field models in curved spacetime. From the perspective of effective field theory (setting renormalization aside), in  $(3+1)$  spacetime dimensions such couplings take the form of operators in the action with mass dimension 4, and hence they should be included unless forbidden by the specific symmetries of a given theory.

In this work we study multifield inflation in the simplest axion model, including the nonminimal coupling of the radial field to gravity. The potential for the axion field, when expressed in the Einstein frame, is exponentially sensitive to the radial field. This leads to dynamics akin to hybrid inflation [26–28], with a phase of inflation driven by the radial field followed by a phase of inflation driven by the axion. This bears a striking resemblance to dynamics recently observed in supergravity [29, 30] and supergravity-inspired [31] multifield models. It is particularly striking that the behavior of this model emerges from such simple ingredients.

Turning to cosmological perturbations, we find a phenomenon recently observed in multifield models with curved field-space manifolds [16, 30–40], namely, ultra-light isocurvature perturbations [41]. In the model developed here, the isocurvature perturbations are ultra-light during the radial-inflation phase, and develop a nearly scale-invariant spectrum of perturbations on large scales. They become super-heavy during the axion-inflation phase, and subsequently rapidly decay. At the interface of these two regimes, there can be a rapid conversion of isocurvature into curvature perturbations, leading to an overall enhancement of the amplitude of the curvature perturbation power spectrum. In the language

of multifield inflation, this system exhibits a turning trajectory with a fast turn.

This has important implications for next-generation cosmic microwave background (CMB) experiments, in particular regarding the observation or non-observation of primordial gravitational waves, since the tensor-to-scalar ratio  $r$  can be suppressed in this scenario due to the relative enhancement of the scalar spectrum. We find that the duration of axion inflation in this scenario is constrained by measurements of the scalar spectral index  $n_s$  to be  $\lesssim 15$  e-folds of expansion, while the suppression of  $r$  can become non-negligible even for modest values of the nonminimal coupling,  $\xi \gtrsim \mathcal{O}(1)$ .

Finally, this scenario has implications for the phenomenology of axions. Considering the axions' canonical interaction with gauge fields, we find the interaction strength during the radial phase is suppressed relative to the interaction strength during the axion-inflation phase. This decouples the constraints on inflationary production of gauge fields (e.g., from primordial black holes) from the constraints on production at (p)reheating.

The remainder of this paper is organized as follows. In Sec. II we introduce the model and identify parameter ranges of interest. We analyze the inflationary background dynamics in Sec. III, and study the evolution of perturbations in Sec. IV. We compute the associated observables and constraints in Sec. V, and in Sec. VI we perform a brief analysis of the interaction with gauge fields. We close in Sec. VII with a discussion of directions for future work.

## II. NONMINIMAL COUPLINGS AND AXIONS

The starting point for this work is the operational definition of the axion field: the pseudo-Nambu-Goldstone boson of a spontaneously broken global  $U(1)$  symmetry, which gains a mass through an explicit symmetry breaking by nonperturbative effects. (See, e.g., Refs. [1–3] for the original works, and Refs. [11–13] for ubiquitous realizations in string theory.) This theory is naturally described in terms of a complex scalar field  $\Phi$ , with the axion  $\vartheta$  defined as the phase of  $\Phi$ :  $\Phi = \varphi e^{i\vartheta}$ .

Self-interacting scalar fields in curved spacetime will generically develop a nonminimal coupling to gravity, acquired through loop effects [17–25]. More generally, the interaction  $|\Phi|^2 R$  is a dimension-4 operator allowed by the symmetries of the problem, and thus, from the perspective of effective field theory, must be included. With this in mind, in this work we generalize the canonical axion model to incorporate a nonminimal coupling of the complex scalar field  $\Phi$  to gravity.

We work in  $(3+1)$  spacetime dimensions and consider an action of the form

$$S_J = \int d^4x \sqrt{-\tilde{g}} \left[ f(\Phi) \tilde{R} - \frac{1}{2} |\partial\Phi|^2 - V(\Phi) \right]. \quad (1)$$

The subscript  $J$  denotes that the action of Eq. (1) is

written in the Jordan frame, in which the nonminimal coupling  $f(\Phi) \tilde{R}$  remains explicit. Given that the axion, by construction, is not subject to perturbative breaking of the  $U(1)$  symmetry, the nonminimal coupling is constrained to depend only on  $|\Phi| \equiv \varphi$ .

The potential for  $\Phi$  consists of two contributions. The spontaneous symmetry breaking (“Higgs”) potential,  $V_{\text{SSB}} = \lambda (|\Phi|^2 - v^2)^2/4$ , ensures that the ground state of the theory is the  $U(1)$  symmetry-breaking state  $\langle |\Phi| \rangle = v$ . In addition, nonperturbative effects generate a potential for the axion field,  $V_a = \Lambda^4 (1 - \cos\vartheta)$ , as in “natural inflation” [42]. The value of  $\Lambda$  is determined by the microphysics of the theory. In QCD constructions, e.g., the Peccei-Quinn axion [1],  $\Lambda^4 = \chi$  is the topological susceptibility of the QCD vacuum (for a review, see, e.g., Ref. [43]). More generally, one might expect  $\Lambda$  to be a function of the radial field  $\varphi$ ; indeed, in string theory constructions this is generally the case (see, e.g., Ref. [13]). For simplicity, we will take  $\Lambda$  to be a constant and a free parameter, constrained only by the requirement that the energy scale of the explicit  $U(1)$  symmetry breaking ( $\Lambda$ ) be lower than the energy scale of spontaneous  $U(1)$  symmetry breaking ( $v$ ).

To simplify the analysis, we decompose  $\Phi$  into real fields as  $\Phi = \varphi e^{i\vartheta}$ . The action then reads

$$S_J = \int d^4x \sqrt{-\tilde{g}} \left[ f(\varphi) \tilde{R} - \frac{1}{2} (\partial\varphi)^2 - \frac{1}{2} \varphi^2 (\partial\vartheta)^2 - \frac{\lambda}{4} (\varphi^2 - v^2)^2 - \Lambda^4 (1 - \cos\vartheta) \right]. \quad (2)$$

The kinetic terms are those of conventional polar coordinates on a flat field space. This defines a metric on the field-space manifold in the Jordan frame,  $\mathcal{G}_{IJ}^{(J)}$ , with components,

$$\mathcal{G}_{\varphi\varphi}^{(J)} = 1 \quad , \quad \mathcal{G}_{\vartheta\vartheta}^{(J)} = \varphi^2, \quad (3)$$

where the superscript  $J$  refers to Jordan frame.

We next perform a conformal transformation of the spacetime metric, to work in the Einstein frame [44, 45]

$$g_{\mu\nu} = \frac{2f}{M_{\text{pl}}^2} \tilde{g}_{\mu\nu}. \quad (4)$$

This serves to make the coupling to gravity canonical; in doing so it modifies both the kinetic and potential terms in the action. The action in the Einstein frame takes the form

$$S_E = \int d^4x \sqrt{-g} \left[ \frac{M_{\text{pl}}^2}{2} R - \frac{1}{2} g^{\mu\nu} \mathcal{G}_{IJ}^{(E)} \partial_\mu \phi^I \partial_\nu \phi^J - V_E(\phi^I) \right], \quad (5)$$

for  $\phi^I = (\varphi, \vartheta)$ . The field-space metric in the Einstein frame becomes

$$\mathcal{G}_{IJ}^{(E)} = \frac{M_{\text{pl}}^2}{2f} \mathcal{G}_{IJ}^{(J)} + \frac{3M_{\text{pl}}^2}{2} \frac{f_{,I} f_{,J}}{f^2}, \quad (6)$$

where  $f_{,I} \equiv \partial f / \partial \phi^I$  denotes a derivative with respect to field  $\phi^I$ . In our simple case, the field-space metric remains diagonal, with the nonvanishing components

$$\mathcal{G}_{\varphi\varphi}^{(E)} = \frac{M_{\text{pl}}^2}{2f} \left( 1 + \frac{3f_{,\varphi}^2}{f} \right), \quad \mathcal{G}_{\vartheta\vartheta}^{(E)} = \frac{M_{\text{pl}}^2}{2f} \varphi^2. \quad (7)$$

The kinetic term of the axion defines the axion decay constant in the Einstein frame,

$$f_a = \frac{\langle \varphi \rangle}{\sqrt{2f}} M_{\text{pl}}. \quad (8)$$

Meanwhile the potential is rescaled, and is given by

$$V_E(\varphi, \vartheta) = M_{\text{pl}}^4 \frac{V(\varphi, \vartheta)}{4f^2(\varphi)}. \quad (9)$$

We consider the usual form of the nonminimal coupling [17–25],

$$f(\varphi) = \frac{1}{2} (M^2 + \xi \varphi^2). \quad (10)$$

To remain consistent with late-time observations, we require  $2f(v) = M_{\text{pl}}^2$  when  $\varphi$  reaches the minimum of its potential,  $\langle \varphi \rangle = v$ . This in turn requires  $M^2 = M_{\text{pl}}^2 - \xi v^2$ . We note that in the ground state,  $\langle \varphi \rangle = v$ , the axion decay constant  $f_a$  of Eq. (8) obeys  $f_a = v$ , independent of  $\xi$  and  $M$ .

The conformal transformation to the Einstein frame transforms the flat field space of the Jordan frame into a *curved* field space [44]. The Ricci scalar of the field-space manifold in the Einstein frame is a function of the radial field  $\varphi$ , as shown in Fig. 1. The full form is given in Appendix A. The curvature is peaked at  $\varphi = 0$ , where it takes a value set by  $\xi$ :  $\mathcal{R}_E = 4\xi(1 + 3\xi)/M_{\text{pl}}^2$ . More generally, one can identify two regimes of interest. To do so, we define the the ratio,

$$r_\varphi \equiv \frac{\sqrt{\xi}\varphi}{M}. \quad (11)$$

For  $r_\varphi \ll 1$ , the curvature can be expanded as

$$\mathcal{R}_E|_{r_\varphi \ll 1} = \frac{4\xi(1 + 3\xi)}{M_{\text{pl}}^2} (1 + \mathcal{O}(r_\varphi^2)), \quad (12)$$

whereas in the opposite regime,  $r_\varphi \gg 1$ , it takes the form

$$\mathcal{R}_E|_{r_\varphi \gg 1} = \frac{4\xi}{M_{\text{pl}}^2(1 + 6\xi)r_\varphi^2} \left( 1 + \mathcal{O}\left(\frac{1}{r_\varphi^2}\right) \right). \quad (13)$$

This has implications even once the radial field has settled into the minimum of its potential,  $\langle \varphi \rangle = v$ . In the limit  $\sqrt{\xi}v \gg M$ ,  $\xi$  held fixed, the vacuum is well approximated by a flat field space ( $\mathcal{R}_E \ll 1/M_{\text{pl}}^2$ ), whereas for  $\sqrt{\xi}v \ll M$ , the field space is curved, even in vacuum.

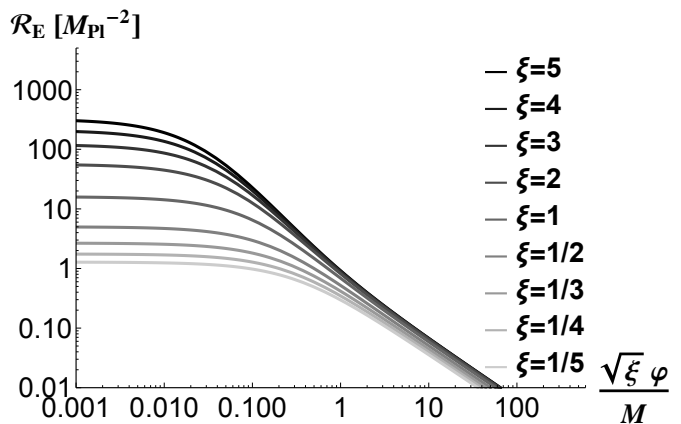


FIG. 1. The Ricci scalar of the field-space manifold in the Einstein frame,  $\mathcal{R}_E$ . This quantity depends only on the radial field  $\varphi$ , and takes the form  $\mathcal{R}_E = f(\xi, r_\varphi)/M_{\text{pl}}^2$  with  $r_\varphi = \sqrt{\xi}\varphi/M$ . The curvature at  $\sqrt{\xi}\varphi/M \ll 1$  is set by  $\xi$ ; in the figure we show  $\mathcal{R}_E$  for  $\xi = 1/5, 1/4, 1/3, 1/2, 1, 2, \dots, 5$  (bottom to top).

The background dynamics follow from the equations of motion for the fields and the Friedmann equation. These can be written,

$$\ddot{\varphi} + 3H\dot{\varphi} + \Gamma_{\varphi\varphi}^\varphi \dot{\varphi}^2 + \Gamma_{\vartheta\vartheta}^\varphi \dot{\vartheta}^2 + \mathcal{G}^{\varphi\varphi} V_{E,\varphi} = 0 \quad (14)$$

$$\ddot{\vartheta} + 3H\dot{\vartheta} + 2\Gamma_{\vartheta\varphi}^\vartheta \dot{\varphi}\dot{\vartheta} + \mathcal{G}^{\vartheta\vartheta} V_{E,\vartheta} = 0, \quad (15)$$

where  $\Gamma_{JK}^I$  denote the Christoffel symbols associated with the field-space metric  $\mathcal{G}_{IJ}^{(E)}$ , given in Appendix A. The Friedmann equation takes the form

$$3M_{\text{pl}}^2 H^2 = \frac{1}{2} \left( \frac{M_{\text{pl}}^2}{2f} \right) \left[ 1 + \frac{6\xi^2 \varphi^2}{2f} \right] \dot{\varphi}^2 + \frac{1}{2} \left( \frac{M_{\text{pl}}^2}{2f} \right) \varphi^2 \dot{\vartheta}^2 + V_E, \quad (16)$$

where the Einstein-frame potential is given by

$$V_E = \frac{\lambda M_{\text{pl}}^4}{4} \frac{(\varphi^2 - v^2)^2}{(M^2 + \xi\varphi^2)^2} + \frac{M_{\text{pl}}^4 \Lambda^4}{(M^2 + \xi\varphi^2)^2} (1 - \cos\vartheta), \quad (17)$$

as per Eq. (9). One can appreciate from Eq. (17) that the change to the Einstein frame, at large  $\varphi$ , flattens the symmetry breaking potential and suppresses the magnitude of the axion potential.

To simplify the analysis of the background dynamics, we consider the length of the background fields' velocity vector [16, 31–40]

$$\dot{\sigma} \equiv |\dot{\varphi}^I| = \sqrt{\mathcal{G}_{IJ}^{(E)}} \dot{\varphi}^I \dot{\varphi}^J, \quad (18)$$

where the components of the vector  $\dot{\varphi}^I(t) = (\dot{\varphi}(t), \dot{\vartheta}(t))$  consist of the derivatives (with respect to cosmic time  $t$ ) of the spatially homogeneous background fields. We may

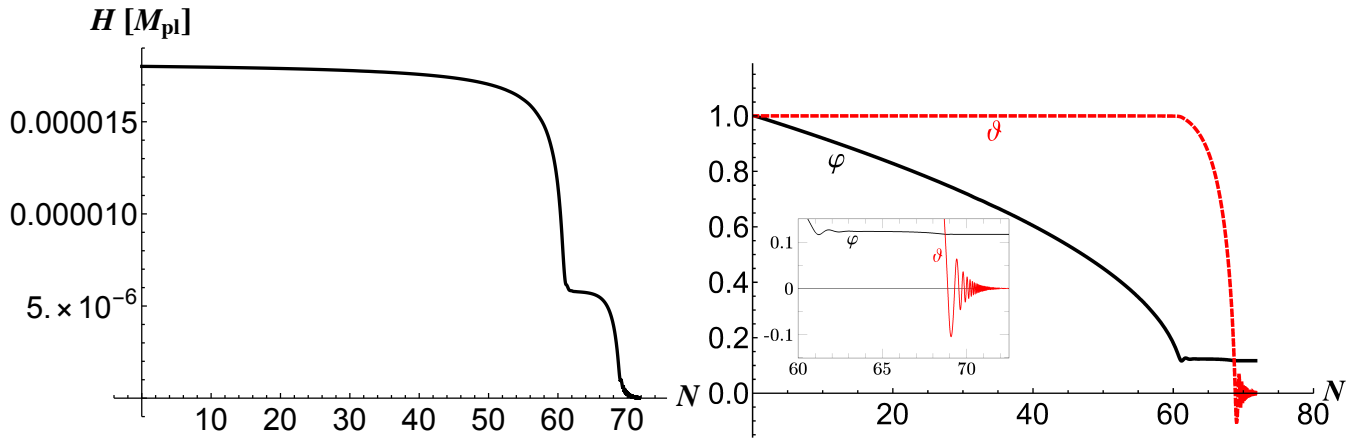


FIG. 2. Evolution of the Hubble parameter (*left*) and the fields  $\varphi$  (black) and  $\vartheta$  (red, dashed) (*right*). (We normalize each field by its initial value.) We set  $\xi = 1$  and  $M = M_{\text{pl}}/10$ , which fixes  $v = \sqrt{99/100} M_{\text{pl}}$ , and take initial conditions  $\varphi_i = 8.5 M_{\text{pl}}$ ,  $\dot{\varphi}_i = 0$ ,  $\vartheta_i = 0.97\pi$ ,  $\dot{\vartheta}_i = 0$ , with  $\lambda = 4 \times 10^{-9}$  and  $\Lambda = 2.74 \times 10^{-3}$ . The insert on the right shows a magnification of the graph, from  $N = 60$  to  $72.5$ . The parameter dependence is illustrated in Figs. 4 and 5.

then define a unit vector that points in the direction of the background fields' evolution:

$$\hat{\sigma}^I \equiv \frac{\dot{\varphi}^I}{\dot{\sigma}}. \quad (19)$$

The background equations simplify to

$$H^2 = \frac{1}{3M_{\text{pl}}^2} \left[ \frac{1}{2} \dot{\sigma}^2 + V_E \right], \quad (20)$$

$$\ddot{\sigma} + 3H\dot{\sigma} + V_{E,\sigma} = 0,$$

where we define

$$V_{E,\sigma} \equiv \hat{\sigma}^I V_{E,I}. \quad (21)$$

Thus we arrive at effectively single-field background evolution, along a direction in field space defined by  $\hat{\sigma}^I$ .

The evolution of the direction of the trajectory can be described by the covariant turn-rate vector,

$$\omega^I \equiv \mathcal{D}_t \hat{\sigma}^I, \quad (22)$$

where  $\mathcal{D}_t A^I \equiv \dot{\varphi}^J \mathcal{D}_J A^I$  for a vector  $A^I$  in the field space, and  $\mathcal{D}_J A^I$  is the usual covariant derivative associated with the field-space metric  $\mathcal{G}_{IJ}^{(E)}$ . We may define the (scalar) turn rate as [46]

$$\omega \equiv \epsilon_{IJ} \hat{\sigma}^I \omega^J, \quad (23)$$

where

$$\epsilon_{IJ} \equiv \left[ \det \left( \mathcal{G}_{IJ}^{(E)} \right) \right]^{1/2} \bar{\epsilon}_{IJ}, \quad \epsilon^{IJ} = \left[ \det \left( \mathcal{G}_{IJ}^{(E)} \right) \right]^{-1/2} \bar{\epsilon}^{IJ}, \quad (24)$$

and  $\bar{\epsilon}_{IJ} = \bar{\epsilon}^{IJ}$  is the usual Levi-Civita symbol:  $\bar{\epsilon}_{12} = +1$  and  $\bar{\epsilon}_{IJ} = -\bar{\epsilon}_{JI}$ . Note that with this definition of the scalar turn rate,  $\omega = \pm |\omega^I|$ .

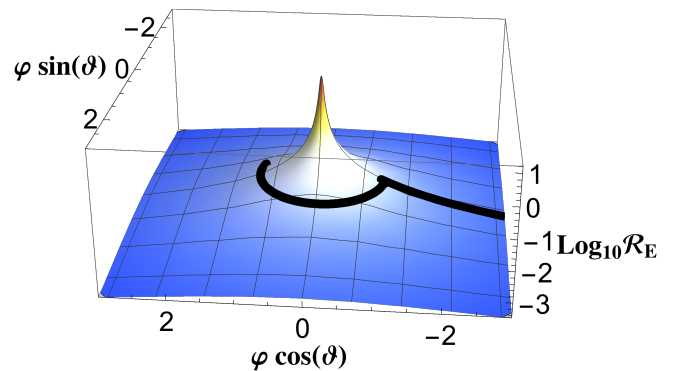


FIG. 3. The inflationary trajectory in field space (black line), for the example parameters of Fig. 2, superimposed on a plot of the field-space Ricci scalar  $\mathcal{R}_E$ . We set  $M_{\text{pl}} = 1$ . For illustrative purposes, only the end of the radial-inflation phase is shown.

### III. THE TWO PHASES OF INFLATION

We assume initial conditions  $\varphi \gg v$ ,  $r_\varphi \gg 1$ , and an initial displacement angle of the axion  $\vartheta \sim \mathcal{O}(1)$ . In this case the potential of Eq. (17) is initially dominated by the radial field  $\varphi$ , and is well approximated by the plateau,

$$V_E \sim \frac{\lambda}{4\xi^2} M_{\text{pl}}^4. \quad (25)$$

As  $\varphi$  decreases towards  $v$ , the axion potential rises to prominence, and can trigger the onset of a second phase of inflation. The relative number of e-folds of radial and axion inflation is controlled by the initial conditions and parameters of the model. A paradigmatic example is shown in Fig. 2, which shows the evolution of the Hubble parameter and the scalar fields for  $\xi = 1$  and  $\vartheta_i = 0.97\pi$ . Two distinct phases of inflationary evolution are evident, with  $N_r \simeq 60$  e-folds of inflation driven by the radial

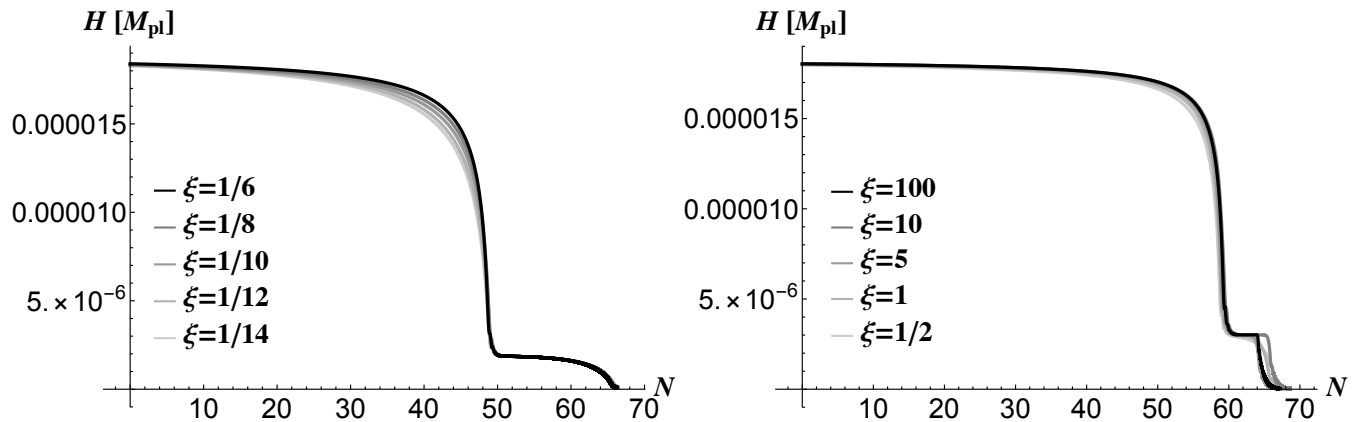


FIG. 4. The dynamics of radial inflation. Smaller values of  $\xi$  accelerate the decline of  $H$  during the radial-inflation phase, as per the slow-roll parameters of Eq. (35). (Left) We fix  $v = 2M_{\text{pl}}$  and vary  $\xi = 1/6, 1/8, 1/10, 1/12,$  and  $1/14$  (top to bottom). The axion initial conditions are  $\vartheta_i = 0.9\pi, \dot{\vartheta}_i = 0$  for all cases, and, for the purpose of visual comparison, we adjust  $\lambda$  to keep  $H_i$  fixed. (Right) To allow for  $\xi \gg 1$  we fix  $\sqrt{\xi}v = (9/10)M_{\text{pl}}$  and vary  $\xi = 100, 10, 5, 1,$  and  $1/2$  (top to bottom). Initial conditions for the axion field are chosen to fix  $N_a \simeq 5$ . The full set of parameters are listed in Appendix B.

field  $\varphi$ , followed by a sudden transition to (in this case)  $N_a \simeq 10$  e-folds of inflation driven by the axion field. In Fig. 3, this inflationary trajectory is shown in field space, superimposed on a plot of the field-space Ricci scalar  $\mathcal{R}_E$ .

This behavior can be understood analytically. Let us first consider the radial field  $\varphi$ . At early times, we have  $f \simeq \frac{1}{2}\xi\varphi^2$ , and hence

$$\ddot{\varphi} + 3H\dot{\varphi} - \frac{\dot{\varphi}^2}{\varphi} + \frac{\xi\varphi^2}{M_{\text{pl}}^2(1+6\xi)}V_{E,\varphi} \simeq 0, \quad (26)$$

where we have neglected the term  $-M^2\dot{\vartheta}^2/[\xi(1+6\xi)]$ , because it is negligibly small in the cases discussed in this paper. In the slow-roll limit, this simplifies further, to

$$3H\dot{\varphi} + \left(\frac{\varphi^2}{6\alpha M_{\text{pl}}^2}\right)V_{E,\varphi} \simeq 0, \quad (27)$$

where we have defined  $\alpha$  as

$$\alpha \equiv 1 + \frac{1}{6\xi}. \quad (28)$$

To make contact with the past literature (see, e.g., Refs. [47, 48]), we define

$$\phi \equiv \sqrt{6\alpha}M_{\text{pl}}\ln(\varphi/M_{\text{pl}}). \quad (29)$$

The slow-roll equation of motion becomes simply

$$3H\dot{\phi} + \partial_{\phi}V_E \simeq 0. \quad (30)$$

Thus we arrive at the standard equation describing single-field slow-roll inflation of a canonically normalized scalar field.

We now turn to the potential. In the regime for which  $f \simeq \frac{1}{2}\xi\varphi^2$ , the potential is given by

$$V_E \simeq \frac{\lambda}{4}M_{\text{pl}}^4\frac{(\varphi^2 - v^2)^2}{\xi^2\varphi^4} + \frac{M_{\text{pl}}^4\Lambda^4}{\xi^2\varphi^4}(1 - \cos\vartheta). \quad (31)$$

In terms of the rescaled radial field  $\phi$ , this may be written

$$V_E \simeq \frac{\lambda}{4}\frac{M_{\text{pl}}^4}{\xi^2}\left(1 - \frac{v^2}{M_{\text{pl}}^2}e^{-\sqrt{\frac{2}{3\alpha}}\phi/M_{\text{pl}}}\right)^2 + \frac{\Lambda^4}{\xi^2}e^{-2\sqrt{\frac{2}{3\alpha}}\phi/M_{\text{pl}}}(1 - \cos\vartheta). \quad (32)$$

By construction, the axion term makes a subdominant contribution in this regime, since it arises from the spontaneous breaking of an approximate symmetry. The phase of inflation driven by the radial field is therefore well approximated as being driven by the first contribution in Eq. (32), which we may write as

$$V_E \simeq V_0\left(1 - \frac{v^2}{M_{\text{pl}}^2}e^{-\sqrt{\frac{2}{3\alpha}}\phi/M_{\text{pl}}}\right)^2, \quad (33)$$

where we define  $V_0 \equiv (\lambda M_{\text{pl}}^4)/(4\xi^2)$ . This form of the potential is familiar as a class of inflation models known as  $\alpha$ -attractors [49–51].

During the slow-roll phase of radial inflation, when  $v^2e^{-\sqrt{\frac{2}{3\alpha}}\phi/M_{\text{pl}}} \ll M_{\text{pl}}^2$ , the radial field  $\varphi$  evolves as

$$\varphi(N) \simeq v\sqrt{\frac{4N}{3\alpha}}, \quad (34)$$

for  $N \gg 1$ , where  $N$  measures the number of e-folds before the end of inflation,  $dN = -Hdt$ . The evolution of the Hubble parameter is described by the (Hubble) slow-roll parameters,  $\epsilon \equiv d(\ln H)/dN$  and  $\eta \equiv 2\epsilon + (2\epsilon)^{-1}(d\epsilon/dN)$ , which, for  $\alpha \ll N$ , take the form

$$\epsilon(N) = \frac{3\alpha}{4N^2}, \quad \eta(N) = \frac{1}{N}. \quad (35)$$

If we were considering a single-field model with the potential in Eq. (33), then the inflationary predictions for

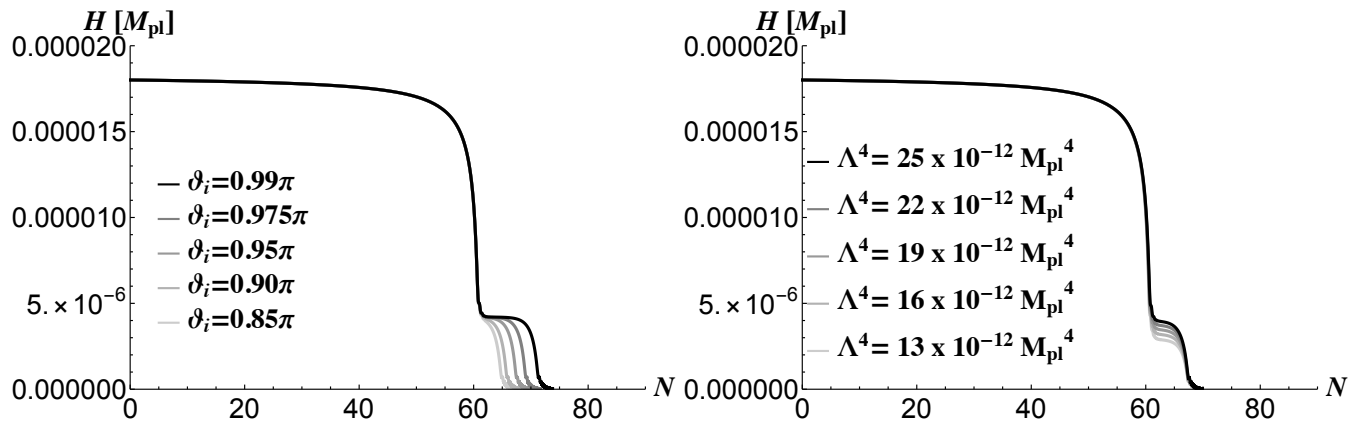


FIG. 5. The dynamics of axion inflation. (*Left*) The number of e-folds of axion inflation,  $N_a$ , is set by the initial condition for the axion field. We consider the example of Fig. 2, but with differing initial conditions,  $\vartheta_i/\pi = 0.85, 0.9, 0.95, 0.975$ , and  $0.99$  (left to right). (*Right*) The energy scale of the axion-inflation phase is set by  $\Lambda$ . We fix  $\vartheta_i = 0.95\pi$  and consider differing values  $\Lambda^4/(10^{-12}M_{\text{pl}}^4) = 25, 22, 19, 16$ , and  $13$  (top to bottom). The full set of parameters are listed in Appendix B.

the spectral index  $n_s$  and tensor-to-scalar ratio  $r$  would follow from these expressions for  $\epsilon$  and  $\eta$ , and be given by

$$n_s = 1 - \frac{2}{N_r}, \quad r = \frac{12\alpha}{N_r^2}, \quad (36)$$

where  $N_r$  is the number of e-folds before the end of radial inflation when the CMB pivot scale exited the horizon. These predictions match those of standard  $\alpha$ -attractor models [31, 40, 50, 52]. In the limit of  $\xi \gg 1$ , or equivalently  $\alpha \rightarrow 1$ , the predictions match those of the Starobinsky model [53], Higgs inflation [47], and, more generally, the attractor behavior of multifield models with nonminimal couplings in the limit  $\xi_I \gg 1$  [54]. However, as we will see in Sec. V, these predictions can be considerably modified in our two-field model, in certain regions of parameter space.

Recalling Eq. (28), which relates  $\alpha$  to  $\xi$ , we see that the evolution of  $\varphi$  encodes the  $\xi$ -dependence of the model. The symmetry-breaking scale  $v$  enters the dynamics as a multiplicative shift of  $\varphi$ , as in Eq. (34), while  $\lambda$  enters only via the height of the plateau  $V_0$ . Thus the dynamics of the radial phase of inflation are determined by  $\xi$ . This can be appreciated from Fig. 4, in which we consider the evolution of the Hubble parameter for differing values of  $\xi$ . In the left panel we fix  $v = 2M_{\text{pl}}$  and the axion initial condition  $\vartheta_i = 0.9\pi$ , and (as usual) adjust  $M$  such that  $\xi v^2 + M^2 = M_{\text{pl}}^2$ , which (for  $v = 2M_{\text{pl}}$ ) requires  $\xi < 1/4$ . In the right panel, we instead fix the combination  $\sqrt{\xi}v = 0.9M_{\text{pl}}$ , which allows us to consider a larger range of values for  $\xi$ .

Now we turn to the axion field. During the phase of radial inflation, the axion is effectively massless, due to the exponential suppression of the axion potential. In particular, since the field-space metric is nearly flat during the radial-inflation phase, the axion mass reduces to  $m_\vartheta^2 \simeq V_{E,\vartheta\vartheta}$ . Compared to the Hubble scale during ra-

dial inflation, we find

$$\frac{|m_\vartheta^2|}{H^2} \simeq \frac{\Lambda^4}{2\xi^2 V_0} e^{-2\sqrt{\frac{2}{3\alpha}}\phi/M_{\text{pl}}} \ll 1. \quad (37)$$

For  $\Lambda^4 < V_0$ , the axion remains ultra-light during radial inflation. In that regime, with  $\xi\varphi^2 \gg M^2$ , we also find  $\Gamma_{\vartheta\varphi}^\vartheta \ll H$ , and hence Eq. (15) reduces to

$$\ddot{\vartheta} + 3H\dot{\vartheta} \simeq 0. \quad (38)$$

During radial inflation, the axion obeys  $|\dot{\vartheta}| \ll H$ , and remains effectively frozen in place.

As  $\varphi$  settles at  $\varphi \approx v$ , the energy density in the axion will eventually dominate, leading to a phase of axion inflation. The number of e-folds of axion inflation is given by [55]

$$N_a \simeq -\frac{v^2}{M_{\text{pl}}^2} \ln \left[ \frac{M_{\text{pl}}^2 + 2v^2}{4v^2} (1 + \cos\vartheta_i) \right], \quad (39)$$

where  $\vartheta_i$  is the value of  $\vartheta$  at the onset of axion inflation. Since  $\vartheta$  undergoes ultra-slow-roll evolution during the radial-inflation phase, the value of  $\vartheta$  at the start of the axion-inflation phase is virtually unchanged from its value at the onset of radial inflation. The dependence of  $N_a$  on  $\vartheta_i$  is shown in the left panel of Fig. 5.

The Hubble parameter during the phase of axion inflation is given by

$$H_a^2 \simeq \frac{2\Lambda^4}{3M_{\text{pl}}^2}. \quad (40)$$

The ratio of the Hubble parameter during axion inflation ( $H_a$ ) to its value during radial inflation ( $H_r$ ) is

$$r_H \equiv \frac{H_a}{H_r} \simeq \frac{\sqrt{2}\Lambda^2}{\sqrt{V_0}}. \quad (41)$$

In the right panel of Fig. 5 we show the evolution of  $H$  for varying values of  $\Lambda$ .

#### IV. PERTURBATIONS

We expand each field about a homogeneous background value,

$$\phi^I(x^\mu) = \varphi^I(t) + \delta\phi^I(x^\mu), \quad (42)$$

with  $I = 1, 2$  corresponding to  $\varphi$  and  $\vartheta$ , respectively. We construct the gauge-invariant Mukhanov-Sasaki variables for the perturbations, which to first order in perturbations read [16]

$$Q^I \equiv \delta\phi^I + \frac{\dot{\varphi}^I}{H}\psi, \quad (43)$$

where  $\psi(x^\mu)$  is the scalar metric perturbation on comoving spatial sections. We may project the vector  $Q^I$  into components parallel and perpendicular to the background fields' motion [56],

$$Q^I = \hat{\sigma}^I Q_\sigma + \epsilon^{IJ} \hat{\sigma}_J Q_s, \quad (44)$$

where (for our two-field model) the adiabatic ( $Q_\sigma$ ) and isocurvature ( $Q_s$ ) perturbations are each scalar quantities. The masses of the perturbations are given by the mass-squared matrix [38]

$$\mathcal{M}^I{}_J \equiv \mathcal{G}_{(E)}^{IK} \mathcal{D}_J \mathcal{D}_K V_E - \mathcal{R}^I{}_{LMJ} \dot{\varphi}^L \dot{\varphi}^M, \quad (45)$$

where  $\mathcal{R}^I{}_{LMJ}$  is the Riemann tensor associated with the field-space metric  $\mathcal{G}_{IJ}^{(E)}$ . We may then identify the canonically normalized comoving curvature perturbation and isocurvature perturbation as [38, 56]

$$\mathcal{R} = \frac{H}{\dot{\sigma}} Q_\sigma, \quad (46)$$

and

$$\mathcal{S} = \frac{H}{\dot{\sigma}} Q_s. \quad (47)$$

The equation of motion for  $Q_\sigma$  is given by [38]

$$\begin{aligned} \ddot{Q}_\sigma + 3H\dot{Q}_\sigma + \left[ \frac{k^2}{a^2} + \mathcal{M}_{\sigma\sigma} - \omega^2 - \frac{1}{M_{\text{pl}}^2 a^3} \frac{d}{dt} \left( \frac{a^3 \dot{\sigma}^2}{H} \right) \right] Q_\sigma \\ = 2 \frac{d}{dt} (\omega Q_s) - 2 \left( \frac{V_{,\sigma}}{\dot{\sigma}} + \frac{\dot{H}}{H} \right) (\omega Q_s), \end{aligned} \quad (48)$$

where  $\omega$  is the covariant turn rate defined in Eq. (23), and  $\mathcal{M}_{\sigma\sigma}$  is given by

$$\mathcal{M}_{\sigma\sigma} \equiv \hat{\sigma}_I \hat{\sigma}^J \mathcal{M}^I{}_J = \hat{\sigma}^I \hat{\sigma}^J \mathcal{D}_I \mathcal{D}_J V_E. \quad (49)$$

Note that the symmetry properties of the Riemann curvature tensor prevent the curvature term in Eq. (45) from contributing to  $\mathcal{M}_{\sigma\sigma}$ , since all four indices are contracted with  $\hat{\sigma}^I$  [38]; this simplification is unique to the adiabatic perturbations and does not occur for the isocurvature perturbations.

Equation (48) becomes more transparent when written in terms of  $\mathcal{R}$  and  $\mathcal{S}$ . For a two-field model, this reads (see, e.g., Ref. [46])

$$\frac{d}{dt} (\dot{\mathcal{R}} - 2\omega\mathcal{S}) + (3+\delta)H (\dot{\mathcal{R}} - 2\omega\mathcal{S}) + \frac{k^2}{a^2} \mathcal{R} = 0, \quad (50)$$

where  $\delta \equiv \dot{\epsilon}/(H\epsilon) = 4\epsilon - 2\eta$ . One can appreciate that  $\mathcal{R}$  is massless, consistent with the conservation of the gauge-invariant curvature perturbation on super-Hubble length-scales in the absence of isocurvature perturbations [56–58]. Indeed, on large scales (making no assumptions about slow-roll or slow-turn evolution of the background fields) one finds the familiar solution,

$$\dot{\mathcal{R}} = 2\omega\mathcal{S}, \quad (51)$$

indicating that the curvature perturbation  $\mathcal{R}$  will only evolve (on super-horizon scales) if the background evolution of the system includes a turn, with  $\omega \neq 0$ .

On the other hand, the isocurvature perturbations are in general massive. The equation of motion for  $Q_s$  in a two-field model is given by [38, 54, 59],

$$\ddot{Q}_s + 3H\dot{Q}_s + \left[ \frac{k^2}{a^2} + \mathcal{M}_{ss} + 3\omega^2 \right] Q_s = 4M_{\text{pl}}^2 \frac{\omega}{\dot{\sigma}} \frac{k^2}{a^2} \psi, \quad (52)$$

where

$$\mathcal{M}_{ss} \equiv \hat{s}^{IJ} \mathcal{M}_{IJ} \quad (53)$$

and  $\hat{s}^{IJ} \equiv \mathcal{G}_{(E)}^{IJ} - \hat{\sigma}^I \hat{\sigma}^J$ . On large scales (again without requiring slow-roll), Eq. (52) reduces to

$$\ddot{Q}_s + 3H\dot{Q}_s + \mu_s^2 Q_s \simeq 0, \quad (54)$$

where  $\mu_s$  is the effective mass of the isocurvature perturbations, given by

$$\mu_s^2 \equiv \mathcal{M}_{ss} + 3\omega^2. \quad (55)$$

From this it follows that massive isocurvature perturbations decay as  $Q_s \propto a^{-3/2}$ , whereas massless isocurvature perturbations effectively freeze-out on super-horizon scales, analogous to the curvature perturbation.

The behavior of  $\mu_s^2$  for our two-field model is shown in Fig. 6, for  $\xi$  in the range  $1/10 \leq \xi \leq 5$ . (Full sets of parameters relevant to the plot are listed in Appendix B.) We note that  $|\mu_s|/H \ll 1$  at early times, whereas  $\mu_s/H \gg 1$  at late times. Each of these examples exhibits a fast turn from radial inflation to axion inflation, as indicated by the evolution of the scalar turn rate  $\omega$  of Eq. (23), shown in Fig. 7.

The evolution of the isocurvature perturbation  $Q_s$  is sensitive to this behavior of  $\mu_s$ . We solve Eq. (52) for modes  $Q_s(k, t)$  that exit the Hubble radius early during the radial-inflation phase. We are interested in the behavior of modes after they have crossed outside the Hubble radius, so we neglect the source term on the right-hand side of Eq. (52), which is suppressed for  $k \ll aH$ .

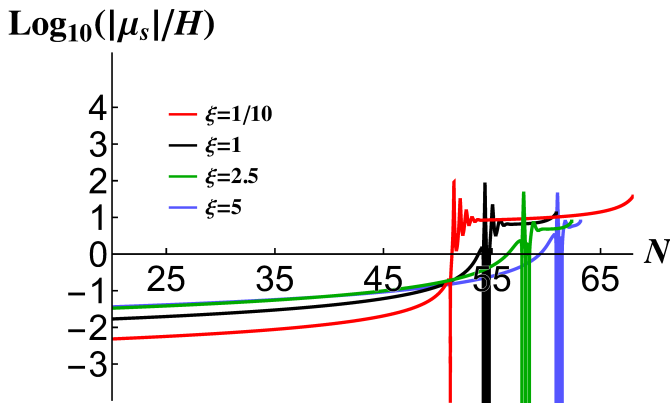


FIG. 6. The ratio of the mass of the isocurvature perturbations to the Hubble parameter,  $|\mu_s|/H$ , for  $\xi = 1/10$  (red),  $\xi = 1$  (black),  $\xi = 2.5$  (green), and  $\xi = 5$  (blue). The mass undergoes a sharp transition from  $|\mu_s| \ll H$  to  $|\mu_s| \gg H$  at the transition from radial to axion-driven inflation. Each curve extends to the end of axion inflation, when  $\epsilon(N_{\text{end}}) = 1$  (which is equivalent to  $\ddot{a}(t_{\text{end}}) = 0$ ). Initial conditions and other parameters for the curves shown here are listed in Appendix B.

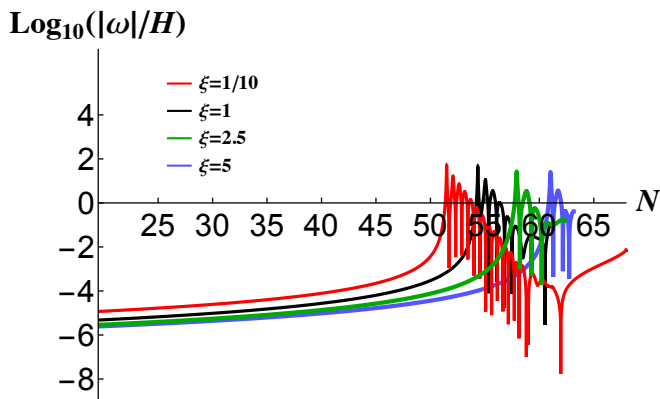


FIG. 7. The ratio of the covariant turn rate to the Hubble parameter,  $|\omega|/H$ , for  $\xi = 1/10$  (red),  $\xi = 1$  (black),  $\xi = 2.5$  (green), and  $\xi = 5$  (blue). The turn rate exhibits a dominant spike and a series of subdominant peaks at the time of the turn from radial to axion inflation. Each curve extends to the end of axion inflation, when  $\epsilon(N_{\text{end}}) = 1$ . Initial conditions and other parameters for the curves shown here are listed in Appendix B. In each case, after the dominant spike the turn rate oscillates through zero, so  $\log(|\omega|/H)$  formally diverges to  $-\infty$ .

The amplitude of modes  $Q_s(k, t)$  freezes soon after Hubble crossing, with amplitude  $Q_{s*}(k)$ . Assuming that the modes begin in the Bunch-Davies vacuum state, and adopting the normalization conventions of Ref. [56], we may approximate the amplitude of these modes as

$$Q_{s*}(k) \simeq \frac{H_*}{\sqrt{2k^3}}, \quad (56)$$

consistent with a (nearly) scale-invariant power spectrum for an effectively massless scalar field. At late

times, after the turn, when  $\mu_s \gg H$ , modes  $Q_s(k, t)$  undergo damped oscillations. At the interface between these regimes, around the time of the turn in field space, long-wavelength modes  $Q_s(k, t)$  undergo a brief period of tachyonic amplification. The mass  $\mu_s$  becomes maximally tachyonic immediately before the turn, as the amplitude of the radial field rapidly decreases, consistent with Eq. (37). See Fig. 8.

The amount by which modes  $Q_s(k, t)$  are amplified around the time of the turn from radial to axion inflation increases with  $\xi$  and with the initial value of the axion field,  $\vartheta_i$ . Around the time of the turn, we may parameterize the amplitude of modes on super-Hubble length-scales as

$$Q_s(k, t_{\text{turn}}) \simeq e^{\mathcal{A}(k)} Q_{s*}(k), \quad (57)$$

where  $\mathcal{A}$  is an amplification factor due to the tachyonic growth. From Eq. (54), we can approximate this as

$$\mathcal{A}(k) \simeq \int dN \frac{|\mu_s^2|}{3H^2}, \quad (58)$$

where the integration is taken over the time period such that  $([k^2/a^2] + \mu_s^2) < 0$ . The magnitude of  $\mathcal{A}(k)$  is correlated both with  $\xi$  and with  $\vartheta_i$ . Before the turn,  $\mu_s^2 \simeq V_{E, \vartheta\vartheta} = (M_{\text{pl}}^4 \Lambda^4 / [M^2 + \xi \varphi^2]^2) \cos \vartheta_i$ , given Eq. (17). Due to the constraint  $M^2 + \xi v^2 = M_{\text{pl}}^2$ , we have  $v < M_{\text{pl}}$  for  $\xi > 1$ . Given Eq. (39), for  $\xi > 1$ , there will only be  $N_a > 0$  e-folds of axion inflation for initial conditions such that  $\cos \vartheta_i \simeq -1$ . Therefore larger values of  $\xi$  correlate with larger values of  $|\mu_s^2|$  around the turn from radial to axion inflation, which generates the largest amplification of modes  $Q_s(k, t)$ . This behavior is consistent with our numerical simulations for the mode with comoving wavenumber  $k_*$  equal to the CMB pivot scale, which we take to be the mode that first crossed outside the Hubble radius 55 e-folds before the end of inflation. The peak values of  $Q_s(k_*, t_{\text{turn}})$  shown in Fig. 8 correspond to  $\mathcal{A}(k_*) \sim 0$  for  $\xi < 1$ ,  $\mathcal{A}(k_*) \sim 1.11$  for  $\xi = 1$ ,  $\mathcal{A}(k_*) = 1.39$  for  $\xi = 2.5$ , and  $\mathcal{A}(k_*) = 3.27$  for  $\xi = 5$ .

From the behavior of modes  $Q_s(k, t)$  we may understand the evolution of  $\mathcal{S}(k, t)$  and, in turn, the effects on curvature perturbations  $\mathcal{R}(k, t)$ . Between the time  $t_*$  that a given mode crosses outside the Hubble radius and the time  $t_{\text{turn}}$  of the turn from radial to axion inflation, we have  $|\omega| \ll H$  and the amplitudes of both  $Q_s(k, t)$  and  $\mathcal{R}(k, t)$  remain effectively frozen. Given Eq. (47), however, modes  $\mathcal{S}(k, t)$  evolve as  $(H/\dot{\sigma}) = 1/(\sqrt{2\epsilon(t)} M_{\text{pl}})$ . For  $t_* < t < t_{\text{turn}}$ , we may therefore write

$$\mathcal{S}(k, t) = \sqrt{\frac{\epsilon_*}{\epsilon(t)}} \mathcal{R}_*(k). \quad (59)$$

Given the growth of  $\epsilon(t)$  during the radial-inflation phase (see Fig. 9), the amplitude of modes  $\mathcal{S}(k, t)$  is suppressed by more than an order of magnitude between  $t_*$  and  $t_{\text{turn}}$ . Around the time of the turn, on the other hand, modes  $Q_s(k, t)$  undergo a tachyonic amplification, as in Eq. (57),

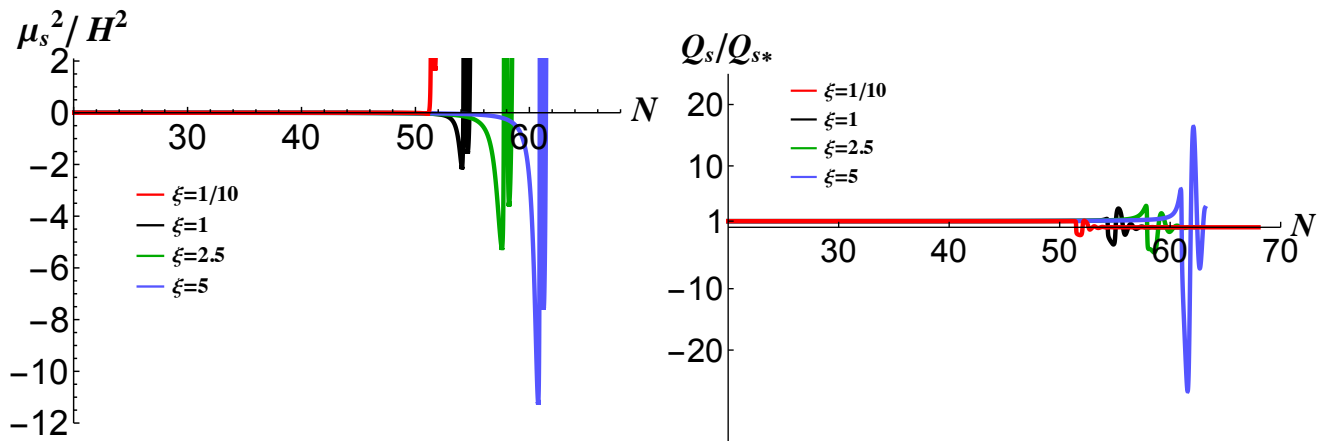


FIG. 8. Evolution of the isocurvature perturbation around the time of the turn in field space. (*Left*) The mass of the isocurvature perturbations becomes maximally tachyonic at the transition from radial to axion inflation, as the radial field rapidly approaches its minimum value,  $\varphi \simeq v$ . (*Right*) The brief period with  $\mu_s^2 < 0$  and  $|\mu_s^2|/H^2 > 1$  amplifies modes  $Q_s(k, t)$  on long length-scales,  $k \ll aH$ , compared to the modes' magnitude following Hubble crossing,  $Q_{s*}$ . The mode shown here has comoving wavenumber  $k_*$  corresponding to the CMB pivot scale, which we take to be the mode  $Q_s(k_*, t)$  that crossed outside the Hubble radius 55 e-folds before the end of inflation. Each curve extends to the end of axion inflation, when  $\epsilon(N_{\text{end}}) = 1$ . Initial conditions and other parameters for the curves shown here are listed in Appendix B.

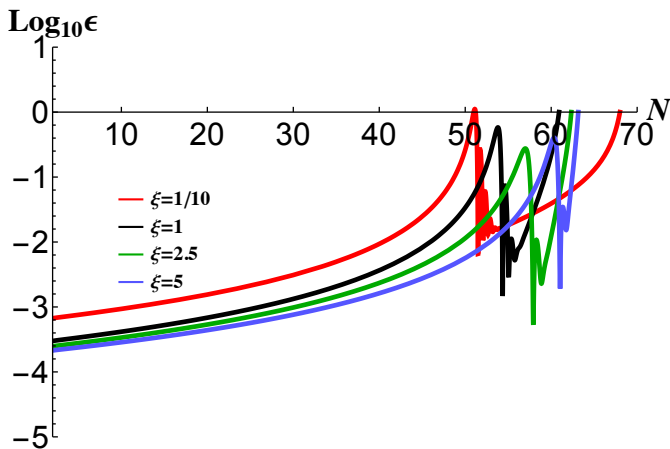


FIG. 9. The slow-roll parameter  $\epsilon = -\dot{H}/H^2$  for  $\xi = 1/10$  (red),  $\xi = 1$  (black),  $\xi = 2.5$  (green), and  $\xi = 5$  (blue). For each value of  $\xi$ , the peak of  $S(k, t)$  around the time of the turn from radial to axion inflation, shown in Fig. 10, corresponds to the first trough in  $\epsilon$ . Initial conditions and other parameters for the curves shown here are listed in Appendix B. Each curve extends to the end of axion inflation, when  $\epsilon(N_{\text{end}}) = 1$ .

which yields an amplification of modes  $S(k, t_{\text{turn}})$  of the form

$$S(k, t_{\text{turn}}) \simeq \sqrt{\frac{\epsilon_*}{\epsilon(t_{\text{turn}})}} e^{\mathcal{A}(k)} \mathcal{R}_*(k), \quad (60)$$

with  $\mathcal{A}(k)$  given in Eq. (58). Moreover, around  $t_{\text{turn}}$ , the slow-roll parameter  $\epsilon(t)$  rapidly reaches a peak and then falls sharply to a trough. The maximum amplitude of  $|S(k, t)|$  corresponds to the trough in  $\epsilon$ , as shown in Fig. 10. Finally, for  $t > t_{\text{turn}}$ ,  $\mu_s^2 \gg H^2$  and hence

$Q_s(k, t)$  as well as  $S(k, t)$  undergo damped oscillations.

From Eq. (51), we may evaluate the effect on the curvature perturbations  $\mathcal{R}(k, t)$ . In general, the change to modes  $\mathcal{R}(k, t)$  for  $k \ll aH$  is given by

$$\Delta\mathcal{R}(k, t) = \int_{t_*}^t dt' 2\omega(t') S(k, t'). \quad (61)$$

Evaluating Eq. (61) numerically for the mode  $k_*$  corresponding to the CMB pivot scale for the cases shown in Figs. 7 - 10, we find  $|\Delta\mathcal{R}(k_*, t_{\text{end}})| \simeq 0$  for  $\xi < 1$ ,  $|\Delta\mathcal{R}(k_*, t_{\text{end}})| \simeq 0.60 \mathcal{R}_*$  for  $\xi = 1$ ,  $|\Delta\mathcal{R}(k_*, t_{\text{end}})| \simeq 2.00 \mathcal{R}_*$  for  $\xi = 2.5$ , and  $|\Delta\mathcal{R}(k_*, t_{\text{end}})| \simeq 5.03 \mathcal{R}_*$ , where  $t_{\text{end}}$  is the end of inflation (at the end of the axion-inflation phase), and  $\mathcal{R}_*$  is the amplitude  $\mathcal{R}(k_*, t_*)$  at the time the mode crossed outside the Hubble radius, during the radial-inflation phase. Full sets of parameters and initial conditions for each of these cases are given in Appendix B.

The power spectrum of curvature perturbations at the end of inflation may be written

$$\mathcal{P}_{\mathcal{R}}(k, N_{\text{end}}) = \left[ 1 + \left( \frac{\Delta\mathcal{R}(k, N_{\text{end}})}{\mathcal{R}_*(k)} \right)^2 \right] \mathcal{P}_{\mathcal{R}}^{(0)}(k), \quad (62)$$

where  $\mathcal{P}_{\mathcal{R}}^{(0)}(k)$  is given by

$$\mathcal{P}_{\mathcal{R}}^{(0)}(k) = \frac{H_*^2}{8\pi^2 M_{\text{pl}}^2 \epsilon_*}, \quad (63)$$

evaluated at the time that the CMB pivot scale crosses outside the Hubble radius. Despite the rapid changes in  $\epsilon$  and  $\omega$  around the time of the turn, there is no discernible change to the spectral index  $n_s$  in this scenario: all modes  $Q_s(k, t)$  of cosmological interest exited the Hubble radius

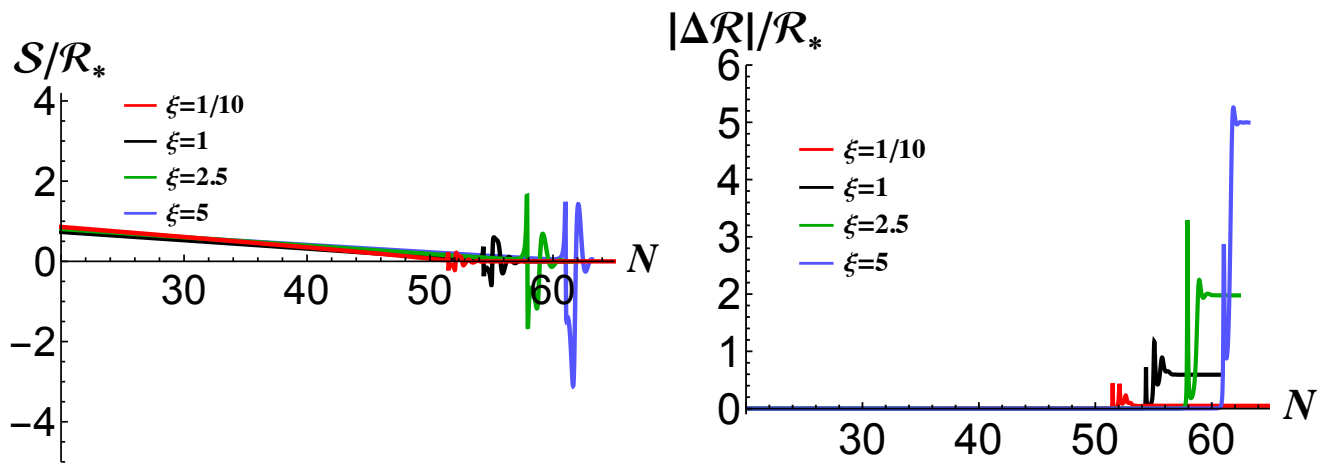


FIG. 10. Evolution of the isocurvature and curvature perturbations between the time of Hubble crossing and the turn from radial to axion inflation, for modes with comoving  $k_*$  corresponding to the CMB pivot scale. There is negligible growth of  $\mathcal{R}(k, t)$  in the  $\xi = 1/10$  (red) and  $\xi = 1$  (black) cases, whereas  $|\Delta\mathcal{R}(k, t)|/\mathcal{R}_*(k) > 1$  for  $\xi = 2.5$  (green) and  $\xi = 5$  (blue). (Here  $\mathcal{R}_*(k)$  is the constant amplitude of the mode following Hubble crossing, before the turn.) Initial conditions and other parameters for the curves shown here are listed in Appendix B. Each curve extends to the end of axion inflation, when  $\epsilon(N_{\text{end}}) = 1$ .

many e-folds before the turn, at times when  $Q_s(k, t)$  and  $Q_\sigma(k, t)$  each evolved as fluctuations of nearly-massless scalar fields. The turn from radial to axion inflation affects all modes with  $k \ll aH$  uniformly.

Similarly, we may evaluate the power spectrum of isocurvature perturbations at late times. Around  $t_*$ , we expect  $\mathcal{P}_S(k, t_*) \simeq \mathcal{P}_R(k, t_*) = \mathcal{P}_R^{(0)}(k)$ , given the similar evolution of  $Q_s(k, t)$  and  $Q_\sigma(k, t)$ . Upon using Eq. (60), the fact that modes  $\mathcal{S}(k, t)$  decay as  $a^{-3/2}(t)$  after the turn (once  $\mu_s^2 \gg H^2$ ), and  $\epsilon(t) \simeq 1$  at the end of axion inflation, we may then estimate

$$\mathcal{P}_S(k, N) \simeq \epsilon_* e^{2A(k)} e^{-3(N_{\text{turn}} - N)} \mathcal{P}_R^{(0)}(k), \quad (64)$$

where  $N_{\text{turn}}$  is the time of the turn and  $N$  is the number of e-folds before the end of inflation. The combination of the slow-roll suppression and the additional suppression during the axion-inflation phase ensures that only a negligible amplitude of isocurvature perturbations remains at the end of inflation. Evaluated at the end of inflation, this is simply

$$\mathcal{P}_S(k, N_{\text{end}}) = \epsilon_* e^{2A(k)} e^{-3N_a} \mathcal{P}_R^{(0)}(k), \quad (65)$$

where  $N_a$  is the number of e-folds of axion inflation.

The growth of modes  $\mathcal{S}(k, t)$  around  $t_{\text{turn}}$  that we have considered here stems largely from tachyonic amplification. For larger values of  $\xi$ , the change of  $\mathcal{S}(k, t)$  could be further enhanced by parametric resonance, as the radial field  $\varphi$  rapidly oscillates around the minimum of its potential,  $\varphi \simeq v$ . Those rapid oscillations would contribute quasi-periodic variations to  $\mu_s^2(t)$ , akin to the resonances studied in preheating in similar multifield models with nonminimal couplings. In general, the strength of such resonances grows with  $\xi$  [60–64], and may become a significant factor for the growth of  $\mathcal{S}(k, t)$  around  $t_{\text{turn}}$  in

this model for  $\xi \gg 1$ . We leave this interesting possibility for future research.

## V. PREDICTIONS AND IMPLICATIONS FOR NEXT GENERATION CMB EXPERIMENTS

We now turn to the observable predictions of the model developed here. The hallmark observables of any inflationary model are the predictions for the scalar spectral index  $n_s$  and for the tensor-to-scalar ratio  $r$ . We first consider the impact of the fast turn on the ratio  $r$ . For the multifield axion model under consideration, the amplitude of the scalar spectrum is rescaled according to Eq. (62). Meanwhile, tensor modes on long length-scales are unaffected by the turn in field space. One can appreciate this from the equation of motion for tensor modes, at linear order in perturbations (see, e.g., Ref. [65]):

$$u_k'' + \left(k^2 - \frac{a''}{a}\right) u_k = 0, \quad (66)$$

where primes denote derivatives with respect to conformal time,  $d\tau = dt/a$ , and  $u_k \equiv ah_k$ , where  $a$  is the scale factor and  $h_k$  is the tensor mode function. Details of the evolution of the background system (including the turn) enter Eq. (66) only through  $a(t)$ . In the limit of long-wavelength perturbations,  $k \rightarrow 0$ , Eq. (66) is solved by  $u_k \propto a$ , and hence constant  $h_k$ . This indicates that  $h_k$  is unaffected by any background evolution that occurs long after the tensor mode with wavenumber  $k$  has exited the horizon. Given the lack of enhancement of tensor modes, the amplitude relative to the scalar perturbations, Eq. (62), is suppressed:

$$r \rightarrow \frac{r}{1 + (\Delta\mathcal{R}/\mathcal{R}_*)^2}, \quad (67)$$

where  $\Delta\mathcal{R}/\mathcal{R}_*$  is shorthand for  $\Delta\mathcal{R}(k, t_{\text{end}})/\mathcal{R}_*(k)$ , and we consider modes with comoving wavenumber near the CMB pivot scale  $k_*$ . For the parameters considered in the previous section, this suppression amounts to roughly a factor of 1.4 for  $\xi = 1$ , 5 for  $\xi = 2.5$  and 26 for  $\xi = 5$ .

In addition to shifting the amplitude of the scalar perturbations, both  $n_s$  and  $r$  are affected by the distinct expansion history in the multifield axion model, which generically includes two phases of inflation rather than only a single phase. In this case, the total number of e-folds of inflationary expansion is different than what one would calculate only for the radial phase of inflation. (See also Refs. [31, 40].) We denote by  $N_*$  the total number of e-folds of inflationary expansion that occur after the CMB pivot scale crosses outside the Hubble radius,  $N_* \equiv N_r + N_a$ . The inflationary predictions then follow from Eqs. (36) and (67):

$$n_s = 1 - \frac{2}{N_* - N_a}, \quad r = \frac{12\alpha}{(N_* - N_a)^2} \frac{1}{1 + (\Delta\mathcal{R}/\mathcal{R}_*)^2}, \quad (68)$$

On the observation side,  $\Lambda$ CDM fit to *Planck* 2018 data combined with BICEP-Keck 2015 and BOSS BAO yields  $n_s = 0.9668 \pm 0.0037$  [66]. Fixing  $N_*$  to be less than the bound  $N_* \lesssim 67$  [67] (see also Refs. [68, 69]), we find that current data fit to minimal  $\Lambda$ CDM are consistent at  $2\sigma$  with  $N_a \lesssim 18$  e-folds of axion inflation. [66]. The bound is considerably weaker if other cosmological parameters are allowed to vary. For example, varying the effective number of neutrino species  $N_{\text{eff}}$  within current bounds allows  $N_a \lesssim 25$ .

Future experiments will significantly improve the sensitivity to  $r$ . With this in mind, in Fig. 11 we show the forecast Simons Observatory constraints on this model when the fast turn is included, using the sensitivity forecasts in Ref. [70]. The grey contours correspond to observations by *Planck* 2018, while the orange and red contours correspond to expected sensitivities of the Simons Observatory. The solid red, black, and blue lines show predictions from a single-field inflationary model with a  $\lambda\varphi^4$  potential and nonminimal coupling  $f(\varphi)$  as in Eq. (10) with  $\xi = 1/10$  (red),  $\xi = 1$  (black),  $\xi = 2.5$  (green), and  $\xi = 5$  (blue), in each case with  $N_*$  ranging from 50 to 60 [71–77]. The dots correspond to predictions from the multifield axion model of Eq. (5) with  $N_* = 60$  (yellow) and 50 (solid red, black, green, and blue), including  $N_a = 1 - 15$  e-folds of axion inflation (increasing from right to left). From this one can appreciate that for a fast turn followed by a small number of e-folds of axion inflation, predictions from the model remain well inside the forecast contours.

As noted in the previous section, the multifield axion model under study produces isocurvature perturbations during inflation as well as (adiabatic) curvature perturbations. The CMB places tight constraints on primordial isocurvature perturbations among  $\Lambda$ CDM components. Whereas inflationary isocurvature perturbations are a necessary condition for observable isocurvature perturbations within the CMB, they are not a sufficient condition.

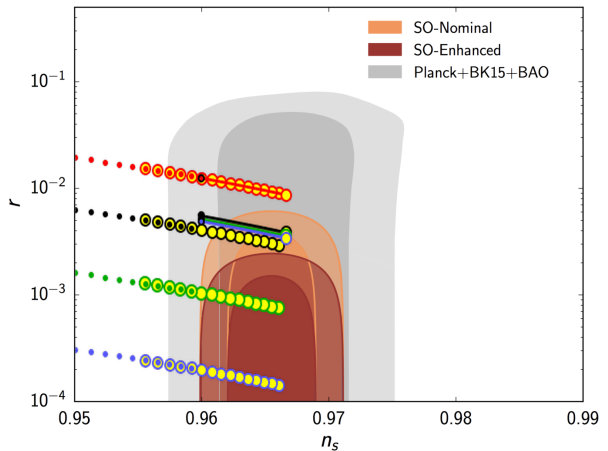


FIG. 11. Simons Observatory forecast for the  $n_s - r$  plane, and constraints on inflation. Image adapted from the Simons Observatory forecast of Ref. [70]. Predictions for  $n_s$  and  $r$  based on Eq. (68) with  $\xi = 1/10$  (red),  $\xi = 1$  (black),  $\xi = 2.5$  (green), and  $\xi = 5$  (blue). Yellow dots indicate predictions for the case in which the CMB pivot scale crossed outside the Hubble radius  $N_* = N_r + N_a = 60$  e-folds before the end of inflation, with dots corresponding to  $N_a = 1, 2, \dots, 14, 15$  e-folds of axion inflation (right to left). Black, red, green, and blue dots denote  $N_* = N_r + N_a = 50$  e-folds of inflation after the CMB pivot scale crossed outside the Hubble radius, with  $N_a = 1, 2, \dots, 14, 15$  e-folds of axion inflation (right to left). The red, black, green, and blue solid lines indicate the predictions from single-field inflation with  $\xi = 1/10, 1, 2.5$ , and 5, respectively, *without* any turn in field space, with  $N_*$  ranging from 50 to 60.

An observable isocurvature fraction also requires that the inflationary isocurvature perturbations be transferred to  $\Lambda$ CDM components. In this context, we may calculate the maximum possible isocurvature fraction that could be observed within the CMB, given the amplification of primordial isocurvature perturbations during inflation. The observed isocurvature fraction will then be bounded by

$$\beta_{\text{iso}}(k) \leq \frac{\mathcal{P}_S(k, N_{\text{end}})}{\mathcal{P}_R(k, N_{\text{end}}) + \mathcal{P}_S(k, N_{\text{end}})}. \quad (69)$$

For the multifield axion model,  $\mathcal{P}_S(k, N_{\text{end}})$  and  $\mathcal{P}_R(k, N_{\text{end}})$  are given by Eqs. (65) and (62), respectively. For this model, we find

$$\beta_{\text{iso}}(k) \lesssim \frac{\epsilon_* e^{2\mathcal{A}(k)} e^{-3N_a}}{1 + \epsilon_* e^{2\mathcal{A}(k)} e^{-3N_a} + [\Delta\mathcal{R}(k, N_{\text{end}})/\mathcal{R}_*(k)]^2} \quad (70)$$

across the range of scales  $k$  relevant for CMB observations. As a conservative example, consider  $N_a = 1$  with  $\epsilon_* = 3.16 \times 10^{-4}$ ,  $\mathcal{A}(k) = 1.39$ , and  $\Delta\mathcal{R}(k, N_{\text{end}})/\mathcal{R}_*(k) = 2.00$ , as in the example with  $\xi = 2.5$  considered in the previous section. In that case, Eq. (70) yields  $\beta_{\text{iso}} \leq 5.1 \times 10^{-5}$ , well below the present bounds from CMB observations [66].

Finally we turn to non-Gaussianity on CMB scales, as parameterized by the amplitude of the bispectrum,  $f_{\text{NL}}$ . As we found in Sec. III, for reasonable choices of parameters and initial conditions this model yields  $N_a \lesssim 15$  e-folds of axion inflation. That means that the fluctuations on CMB scales crossed outside the Hubble radius deep within the radial-inflation phase, prior to the fast turn and onset of axion inflation. Since both curvature perturbations and isocurvature perturbations were massless at the time they first crossed outside the Hubble radius, no non-Gaussianity should be generated in this model beyond the usual, slow-roll suppressed contribution.

The lack of sizeable non-Gaussianity in ultra-light isocurvature scenarios has been emphasized in many recent works, e.g., Refs. [46, 78–80]. We leave a complete calculation of  $f_{\text{NL}}$ , which although unobservably small may differ in form from the single-field result [78], to future work.

An additional feature of the fast turn in field space that may yield an observable signal would be a short-lived oscillation of  $a(t)$  associated with the rapid turn. Such “primordial standard clock” features [81–86] might be observable in the high multipoles of the CMB spectrum, and remain the subject of further research.

## VI. IMPLICATIONS FOR GAUGE FIELD PRODUCTION

The canonical interaction of an axion field is with gauge fields [43]. The interaction can be written in component form as

$$S_{\text{int}} = \frac{\hat{\alpha}}{4} \int d^4x \sqrt{-g} \vartheta F_{\mu\nu} \tilde{F}^{\mu\nu}, \quad (71)$$

where  $\vartheta$  is the axion field,  $\hat{\alpha}$  is the interaction strength (not to be confused with the parameter  $\alpha$  defined in Eq. (28)),  $F_{\mu\nu} = \partial_\mu A_\nu - \partial_\nu A_\mu$  is the gauge field strength, and  $\tilde{F}^{\mu\nu} \equiv \epsilon^{\mu\nu\rho\sigma} F_{\rho\sigma}$ . Despite the explicit factor of  $\sqrt{-g}$  appearing in Eq. (71), the interaction is actually invariant under conformal rescalings of the metric. This implies that the coupling between the axion and the gauge field is *not* rescaled by the conformal factor, even after performing the transformation  $\tilde{g}_{\mu\nu} \rightarrow g_{\mu\nu}$ .

There is a vast literature on the phenomenology of an interaction of the form given in Eq. (71) during inflation. The equation of motion for gauge-field fluctuations is (see, e.g., Refs. [10, 87–89])

$$\frac{d^2 A_{k\pm}}{d\tau^2} + \left( k^2 \pm 2k \frac{\kappa}{\tau} \right) A_{k\pm} = 0, \quad (72)$$

where  $\pm$  denote the two polarizations of the gauge field,  $\tau$  is conformal time ( $d\tau = dt/a$ ),  $k$  is the comoving wavenumber, and  $\kappa$  is given by

$$\kappa = \frac{\hat{\alpha} |\dot{\vartheta}|}{2H}, \quad (73)$$

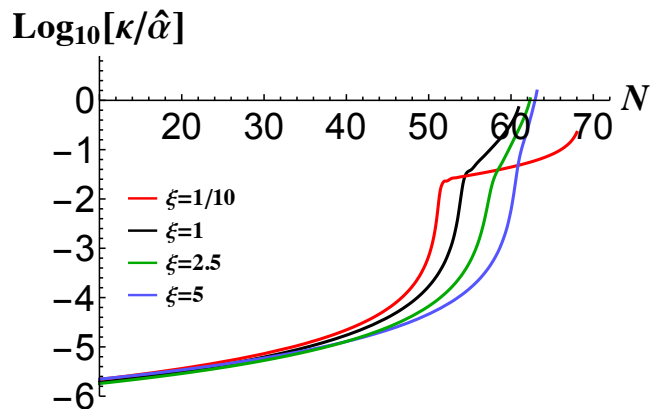


FIG. 12. Evolution of the interaction strength of the axion field to gauge fields,  $\kappa$ , normalized by the coupling constant  $\hat{\alpha}$ , for  $\xi = 1/10$  (red),  $\xi=1$  (black),  $\xi=2.5$  (green), and  $\xi = 5$  (blue). The interaction strength during the axion-inflation phase is orders of magnitude larger than its value during the radial-inflation phase.

where the dot denotes a derivative with respect to cosmic time,  $t$ .

The equation of motion exhibits a tachyonic instability on large scales, for modes satisfying

$$k - \frac{2\kappa}{|\tau|} \leq 0. \quad (74)$$

Due to the  $k$  dependence of the effective mass in Eq. (72), the tachyonic instability is strongest at exactly the moment of horizon crossing, which occurs when the inequality of Eq. (74) is saturated. This is reflected in the solution to Eq. (72), which on large scales is given by [87]

$$A_{k+} = \frac{1}{\sqrt{2k}} \left( \frac{k}{2\kappa_* aH} \right)^{1/4} e^{\pi\kappa_* - 2\kappa_* \sqrt{2k/(\kappa_* aH)}}, \quad (75)$$

$$A_{k-} \simeq 0. \quad (76)$$

The + polarization state is amplified by a factor of  $e^{\pi\kappa_*}$ , where  $\kappa_*$  is  $\kappa$  evaluated at the moment a mode  $k$  entered the tachyonic regime of Eq. (74). The amount of amplification of the mode  $A_{k+}$  is therefore controlled by the parameter  $\kappa$ . We plot the evolution of  $\kappa$ , normalized by  $\hat{\alpha}$ , in Fig. 12. The interaction strength during the axion-inflation phase is orders of magnitude larger than the strength during the radial-inflation phase.

The production of gauge fields in this manner during inflation is constrained by primordial black holes [90] and CMB non-Gaussianity. These constraints apply to modes with comoving wavenumbers  $k$  that exited the horizon at the early and late times during inflation, respectively. Interestingly, neither constraint applies to modes that exited the horizon during the last 10 e-folds of inflation [90], which is precisely the regime of strong gauge-field production identified here.

In contrast, as discussed in detail in Refs. [91, 92], there are tight constraints on the production of gauge fields

after inflation, namely, during preheating. In the present model, these constraints are decoupled from the system's evolution during the phase of radial inflation. We leave a detailed study of preheating in this model to future work.

## VII. DISCUSSION

In this paper we have studied the multifield dynamics of axion inflationary models. Starting from fairly generic ingredients — a complex scalar field, a nonminimal coupling, and the typical potential for an axion field — we have identified an interacting two-field inflationary model. Given that axion models are inherently multifield, and that nonminimal couplings are an inevitable feature of self-interacting scalar fields in curved spacetime, this scenario captures features that we expect to be common across axion-inflation models.

The inflationary dynamics exhibit a sharp transition between phases of inflation predominantly driven by the radial and axion fields, respectively. The dynamics of the first (radial) inflation phase are controlled by the nonminimal coupling  $\xi$ , whereas the dynamics of the second (axion) inflation phase are set by the axion decay constant and the axion field's initial condition. The hierarchy of Hubble parameters during the two phases is determined by the hierarchy of couplings associated with the symmetry-breaking potential for the radial field and with the nonperturbative potential of the axion field.

Cosmological perturbations in this model are readily studied using the covariant formalism of Refs. [16, 32–38], which allows for a straightforward calculation of the conversion of isocurvature perturbations into curvature perturbations, in terms of the integrated covariant turn rate of the background fields' trajectory during the inflationary evolution. From this we find an enhancement of the amplitude of the primordial curvature perturbation spectrum on super-Hubble length-scales, up to  $\mathcal{O}(25)$  for  $\xi = 5$ , generated by the conversion of isocurvature perturbations into curvature perturbations at the rapid transition from radial to axion inflation. We further find an exponential suppression of isocurvature perturbations following the transition,  $\mathcal{P}_S \propto e^{-3N_a}$ , where  $N_a$  is the number of e-folds of axion inflation.

On the other hand, the tensor perturbations on long length-scales remain unaffected by the rapid turn in field space, and hence the tensor-to-scalar ratio  $r$  is suppressed by the relative amplification of the scalar curvature perturbations. The predictions for observables such as the spectral index  $n_s$  and the tensor-to-scalar ratio  $r$  are shifted to sit well inside the forecasted sensitivity of the Simons Observatory, see Fig. 11. This implies that values of the nonminimal coupling  $\xi$  that might naively be ruled out by a non-observation of primordial gravitational waves — such as single-field models with  $\xi = 5$ , which suggest a tensor-to-scalar ratio  $r \sim 3 - 5 \times 10^{-3}$  — would remain consistent with observations once the multifield dynamics, including the fast turn in field space,

are taken into account.

There are many additional avenues of interest regarding the multifield dynamics of axion inflation. Our analysis has focused solely on the predictions for perturbations on CMB scales, namely long-wavelength perturbations, and we have not considered the behavior of modes that exit the horizon around the time of the fast turn. The evolution of such modes is known to generate a spike in the power spectrum, which can be relevant to the production of primordial black holes [30, 41], and other phenomena, such as CMB spectral distortions [93, 94]. In addition, we have identified two distinct phases for the effective interaction strength between the axion field and gauge fields, which remains suppressed during the first (radial) phase of inflation but grows rapidly around the time of the turn to axion inflation. This behavior effectively decouples observable constraints on gauge-field production during inflation from constraints during the preheating era. A more detailed study of the phenomenology of gauge-field production in this model, including predictions for the spectrum of primordial black holes and the gravitational wave signature as well as the dynamics of preheating [88, 95, 96], remain subjects for further research.

## ACKNOWLEDGMENTS

The authors thank Stephon Alexander, Mustafa Amin, Tom Giblin, Mark Hertzberg, and Dong-Gang Wang for helpful discussions. EM is supported in part by a Banting Fellowship from the government of Canada. This research was conducted in MIT's Center for Theoretical Physics and supported in part by the U.S. Department of Energy under Contract No. DE-SC0012567.

## Appendix A: Field Space Quantities

In the Einstein frame, the nonvanishing components of the field-space metric are given in Eq. (7). Upon using Eq. (10) for the nonminimal coupling function  $f(\varphi)$ , we find the nonvanishing components of the Christoffel symbols associated with  $\mathcal{G}_{IJ}^{(E)}$ :

$$\begin{aligned}\Gamma_{\varphi\varphi}^{\varphi} &= \frac{\xi\varphi}{2fC} [6\xi M^2 - C], \\ \Gamma_{\vartheta\vartheta}^{\varphi} &= -\frac{M^2\varphi}{C}, \\ \Gamma_{\vartheta\varphi}^{\vartheta} &= \frac{M^2}{2f\varphi},\end{aligned}\tag{A1}$$

where we have defined the term

$$C \equiv 2f + 6\xi^2\varphi^2.\tag{A2}$$

The Ricci scalar of the field-space manifold in the Einstein frame is given by

$$\mathcal{R}_E(\varphi) = \frac{4\xi[1 + 3\xi + (1 + 6\xi)r_\varphi^2]}{M_{\text{pl}}^2[1 + (1 + 6\xi)r_\varphi^2]^2}, \quad (\text{A3})$$

where

$$r_\varphi \equiv \frac{\sqrt{\xi}\varphi}{M}. \quad (\text{A4})$$

## Appendix B: Parameters for Examples Shown in the Figures

Fig 4, left panel:

$$\begin{aligned} \xi &= 1/6, 1/8, 1/10, 1/12, 1/14 \\ v/M_{\text{pl}} &= 2 \\ 10^{11}\lambda &= 11.9, 6.75, 4.35, 3.04, 2.25 \\ 10^3\Lambda/M_{\text{pl}} &= 1.53 \\ \varphi_i/M_{\text{pl}} &= 14.5, 15.5, 16.2, 16.7, 17.1 \\ \vartheta_i/\pi &= 0.9 \end{aligned}$$

Fig 4, right panel:

$$\begin{aligned} \xi &= 100, 10, 5, 1, 1/2 \\ v/M_{\text{pl}} &= \frac{9}{10\sqrt{\xi}} \\ 10^9\lambda &= 4\xi^2 \\ 10^3\Lambda/M_{\text{pl}} &= 1.93 \\ \varphi_i/M_{\text{pl}} &= 0.90, 2.84, 3.97, 8.37, 11.1 \\ \vartheta_i/\pi &= 1 - 10^{-25}, 1 - 10^{-8}, 1 - 10^{-4}, 0.97, 0.90 \end{aligned}$$

Fig 5, left panel:

$$\begin{aligned} \xi &= 1 \\ v/M_{\text{pl}} &= \sqrt{\frac{99}{100}} \\ 10^9\lambda &= 4\xi^2 \\ 10^3\Lambda/M_{\text{pl}} &= 2.3 \\ \varphi_i/M_{\text{pl}} &= 8.5 \\ \vartheta_i/\pi &= 0.99, 0.975, 0.95, 0.9, 0.85 \end{aligned}$$

Fig 5, right panel:

$$\xi = 1$$

$$\begin{aligned} v/M_{\text{pl}} &= \sqrt{\frac{99}{100}} \\ 10^9\lambda &= 4\xi^2 \\ 10^3\Lambda/M_{\text{pl}} &= 2.24, 2.17, 2.09, 2.00, 1.90 \\ \varphi_i/M_{\text{pl}} &= 8.5 \\ \vartheta_i/\pi &= 0.95 \end{aligned}$$

Examples for Fig 6-11:

Red:

$$\begin{aligned} \xi &= 1/10 \\ v/M_{\text{pl}} &= 3.159 \\ 10^{11}\lambda &= 4.185 \\ 10^3\Lambda/M_{\text{pl}} &= 2.34 \\ \varphi_i/M_{\text{pl}} &= 17 \\ \vartheta_i/\pi &= 0.7 \end{aligned}$$

Black:

$$\begin{aligned} \xi &= 1 \\ v/M_{\text{pl}} &= 0.995 \\ 10^9\lambda &= 4 \\ 10^3\Lambda/M_{\text{pl}} &= 3.03 \\ \varphi_i/M_{\text{pl}} &= 8.0 \\ \vartheta_i/\pi &= 0.96 \end{aligned}$$

Green:

$$\begin{aligned} \xi &= 2.5 \\ v/M_{\text{pl}} &= 0.632 \\ 10^9\lambda &= 25 \\ 10^3\Lambda/M_{\text{pl}} &= 3.60 \\ \varphi_i/M_{\text{pl}} &= 5.41 \\ \vartheta_i/\pi &= 0.99 \end{aligned}$$

Blue:

$$\begin{aligned} \xi &= 5 \\ v/M_{\text{pl}} &= 0.447 \\ 10^9\lambda &= 100 \\ 10^3\Lambda/M_{\text{pl}} &= 3.35 \\ \varphi_i/M_{\text{pl}} &= 4 \\ \vartheta_i/\pi &= 0.99 \end{aligned}$$

- 
- [1] R. D. Peccei and H. R. Quinn, *CP Conservation in the Presence of Instantons*, *Phys. Rev. Lett.* **38** (1977) 1440.
- [2] F. Wilczek, *Problem of Strong P and T Invariance in the Presence of Instantons*, *Phys. Rev. Lett.* **40** (1978) 279.
- [3] S. Weinberg, *A New Light Boson?*, *Phys. Rev. Lett.* **40** (1978) 223.
- [4] K. Freese, J. A. Frieman and A. V. Olinto, *Natural inflation with pseudo - Nambu-Goldstone bosons*, *Phys. Rev. Lett.* **65** (1990) 3233.
- [5] L. McAllister, E. Silverstein and A. Westphal, *Gravity Waves and Linear Inflation from Axion Monodromy*, *Phys. Rev.* **D82** (2010) 046003 [0808.0706].
- [6] E. Silverstein and A. Westphal, *Monodromy in the CMB: Gravity Waves and String Inflation*, *Phys. Rev.* **D78** (2008) 106003 [0803.3085].

- [7] J. Preskill, M. B. Wise and F. Wilczek, *Cosmology of the Invisible Axion*, *Phys. Lett.* **B120** (1983) 127.
- [8] L. F. Abbott and P. Sikivie, *A Cosmological Bound on the Invisible Axion*, *Phys. Lett.* **B120** (1983) 133.
- [9] M. Dine and W. Fischler, *The Not So Harmless Axion*, *Phys. Lett.* **B120** (1983) 137.
- [10] N. Barnaby, E. Pajer and M. Peloso, *Gauge Field Production in Axion Inflation: Consequences for Monodromy, non-Gaussianity in the CMB, and Gravitational Waves at Interferometers*, *Phys. Rev. D* **85** (2012) 023525 [1110.3327].
- [11] P. Svrcek and E. Witten, *Axions In String Theory*, *JHEP* **06** (2006) 051 [hep-th/0605206].
- [12] A. Arvanitaki, S. Dimopoulos, S. Dubovsky, N. Kaloper and J. March-Russell, *String Axiverse*, *Phys. Rev. D* **81** (2010) 123530 [0905.4720].
- [13] M. Cicoli, M. Goodsell and A. Ringwald, *The type IIB string axiverse and its low-energy phenomenology*, *JHEP* **10** (2012) 146 [1206.0819].
- [14] D. Wands, *Multiple field inflation*, *Lect. Notes Phys.* **738** (2008) 275 [astro-ph/0702187].
- [15] X. Chen, *Primordial Non-Gaussianities from Inflation Models*, *Adv. Astron.* **2010** (2010) 638979 [1002.1416].
- [16] J.-O. Gong, *Multi-field inflation and cosmological perturbations*, *Int. J. Mod. Phys. D* **26** (2016) 1740003 [1606.06971].
- [17] N. Chernikov and E. Tagirov, *Quantum theory of scalar fields in de Sitter space-time*, *Ann. Inst. H. Poincaré Phys. Theor. A* **9** (1968) 109.
- [18] J. Callan, Curtis G., S. R. Coleman and R. Jackiw, *A New improved energy - momentum tensor*, *Annals Phys.* **59** (1970) 42.
- [19] T. Bunch, P. Panangaden and L. Parker, *On renormalization of  $\lambda\phi^4$  field theory in curved space-time, I*, *J. Phys. A* **13** (1980) 901.
- [20] T. Bunch and P. Panangaden, *On renormalization of  $\lambda\phi^4$  field theory in curved space-time, II*, *J. Phys. A* **13** (1980) 919.
- [21] N. Birrell and P. Davies, *Quantum Fields in Curved Space*. Cambridge Univ. Press, Cambridge, UK, 1982, 10.1017/CBO9780511622632.
- [22] S. D. Odintsov, *Renormalization Group, Effective Action and Grand Unification Theories in Curved Space-time*, *Fortsch. Phys.* **39** (1991) 621.
- [23] I. Buchbinder, S. Odintsov and I. Shapiro, *Effective action in quantum gravity*. Taylor and Francis, New York, 1992.
- [24] L. E. Parker and D. Toms, *Quantum Field Theory in Curved Spacetime: Quantized Field and Gravity*. Cambridge University Press, New York, 2009, 10.1017/CBO9780511813924.
- [25] T. Markkanen and A. Tranberg, *A Simple Method for One-Loop Renormalization in Curved Space-Time*, *JCAP* **08** (2013) 045 [1303.0180].
- [26] A. D. Linde, *Axions in inflationary cosmology*, *Phys. Lett. B* **259** (1991) 38.
- [27] A. D. Linde, *Hybrid inflation*, *Phys. Rev. D* **49** (1994) 748 [astro-ph/9307002].
- [28] E. J. Copeland, A. R. Liddle, D. H. Lyth, E. D. Stewart and D. Wands, *False vacuum inflation with Einstein gravity*, *Phys. Rev. D* **49** (1994) 6410 [astro-ph/9401011].
- [29] A. Linde, D.-G. Wang, Y. Welling, Y. Yamada and A. Achúcarro, *Hypernatural inflation*, *JCAP* **07** (2018) 035 [1803.09911].
- [30] Y. Aldabergenov, A. Addazi and S. V. Ketov, *Primordial black holes from modified supergravity*, **2006.16641**.
- [31] P. Christodoulidis, D. Roest and E. I. Sfakianakis, *Angular inflation in multi-field  $\alpha$ -attractors*, *JCAP* **11** (2019) 002 [1803.09841].
- [32] S. Groot Nibbelink and B. van Tent, *Density perturbations arising from multiple field slow roll inflation*, **hep-ph/0011325**.
- [33] S. Groot Nibbelink and B. van Tent, *Scalar perturbations during multiple field slow-roll inflation*, *Class. Quant. Grav.* **19** (2002) 613 [hep-ph/0107272].
- [34] D. Seery and J. E. Lidsey, *Primordial non-Gaussianities from multiple-field inflation*, *JCAP* **09** (2005) 011 [astro-ph/0506056].
- [35] D. Langlois and S. Renaux-Petel, *Perturbations in generalized multi-field inflation*, *JCAP* **04** (2008) 017 [0801.1085].
- [36] C. M. Peterson and M. Tegmark, *Testing Two-Field Inflation*, *Phys. Rev. D* **83** (2011) 023522 [1005.4056].
- [37] J.-O. Gong and T. Tanaka, *A covariant approach to general field space metric in multi-field inflation*, *JCAP* **03** (2011) 015 [1101.4809].
- [38] D. I. Kaiser, E. A. Mazenc and E. I. Sfakianakis, *Primordial Bispectrum from Multifield Inflation with Nonminimal Couplings*, *Phys. Rev. D* **87** (2013) 064004 [1210.7487].
- [39] P. Christodoulidis, D. Roest and E. I. Sfakianakis, *Attractors, Bifurcations and Curvature in Multi-field Inflation*, **1903.03513**.
- [40] P. Christodoulidis, D. Roest and E. I. Sfakianakis, *Scaling attractors in multi-field inflation*, *JCAP* **12** (2019) 059 [1903.06116].
- [41] G. A. Palma, S. Sypsas and C. Zenteno, *Seeding primordial black holes in multi-field inflation*, **2004.06106**.
- [42] F. C. Adams, J. Bond, K. Freese, J. A. Frieman and A. V. Olinto, *Natural inflation: Particle physics models, power law spectra for large scale structure, and constraints from COBE*, *Phys. Rev. D* **47** (1993) 426 [hep-ph/9207245].
- [43] PARTICLE DATA GROUP collaboration, M. Tanabashi, K. Hagiwara, K. Hikasa, K. Nakamura, Y. Sumino, F. Takahashi et al., *Review of particle physics*, *Phys. Rev. D* **98** (2018) 030001.
- [44] D. I. Kaiser, *Conformal Transformations with Multiple Scalar Fields*, *Phys. Rev. D* **81** (2010) 084044 [1003.1159].
- [45] H. Abedi and A. M. Abbassi, *Gravitational constant in multiple field gravity*, *JCAP* **05** (2015) 026 [1411.4854].
- [46] A. Achúcarro, V. Atal, C. Germani and G. A. Palma, *Cumulative effects in inflation with ultra-light entropy modes*, *JCAP* **02** (2017) 013 [1607.08609].
- [47] F. L. Bezrukov and M. Shaposhnikov, *The Standard Model Higgs boson as the inflaton*, *Phys. Lett. B* **659** (2008) 703 [0710.3755].
- [48] M. Galante, R. Kallosh, A. Linde and D. Roest, *Unity of Cosmological Inflation Attractors*, *Phys. Rev. Lett.* **114** (2015) 141302 [1412.3797].
- [49] S. Ferrara, R. Kallosh, A. Linde and M. Porrati, *Minimal Supergravity Models of Inflation*, *Phys. Rev. D* **88** (2013) 085038 [1307.7696].
- [50] R. Kallosh, A. Linde and D. Roest, *Superconformal*

- Inflationary  $\alpha$ -Attractors*, *JHEP* **11** (2013) 198 [[1311.0472](#)].
- [51] R. Kallosh, A. Linde and D. Roest, *Large field inflation and double  $\alpha$ -attractors*, *JHEP* **08** (2014) 052 [[1405.3646](#)].
- [52] R. Kallosh and A. Linde, *Planck, LHC, and  $\alpha$ -attractors*, *Phys. Rev. D* **91** (2015) 083528 [[1502.07733](#)].
- [53] A. A. Starobinsky, *A New Type of Isotropic Cosmological Models Without Singularity*, *Adv. Ser. Astrophys. Cosmol.* **3** (1987) 130.
- [54] D. I. Kaiser and E. I. Sfakianakis, *Multifield Inflation after Planck: The Case for Nonminimal Couplings*, *Phys. Rev. Lett.* **112** (2014) 011302 [[1304.0363](#)].
- [55] J. Martin, C. Ringeval and V. Vennin, *Encyclopaedia Inflationaris*, *Phys. Dark Univ.* **5-6** (2014) 75 [[1303.3787](#)].
- [56] C. Gordon, D. Wands, B. A. Bassett and R. Maartens, *Adiabatic and entropy perturbations from inflation*, *Phys. Rev. D* **63** (2000) 023506 [[astro-ph/0009131](#)].
- [57] D. Wands, K. A. Malik, D. H. Lyth and A. R. Liddle, *A New approach to the evolution of cosmological perturbations on large scales*, *Phys. Rev. D* **62** (2000) 043527 [[astro-ph/0003278](#)].
- [58] L. Senatore and M. Zaldarriaga, *The constancy of  $\zeta$  in single-clock Inflation at all loops*, *JHEP* **09** (2013) 148 [[1210.6048](#)].
- [59] K. Schutz, E. I. Sfakianakis and D. I. Kaiser, *Multifield Inflation after Planck: Isocurvature Modes from Nonminimal Couplings*, *Phys. Rev. D* **89** (2014) 064044 [[1310.8285](#)].
- [60] M. P. DeCross, D. I. Kaiser, A. Prabhu, C. Prescod-Weinstein and E. I. Sfakianakis, *Preheating after Multifield Inflation with Nonminimal Couplings, I: Covariant Formalism and Attractor Behavior*, *Phys. Rev. D* **97** (2018) 023526 [[1510.08553](#)].
- [61] M. P. DeCross, D. I. Kaiser, A. Prabhu, C. Prescod-Weinstein and E. I. Sfakianakis, *Preheating after multifield inflation with nonminimal couplings, II: Resonance Structure*, *Phys. Rev. D* **97** (2018) 023527 [[1610.08868](#)].
- [62] M. P. DeCross, D. I. Kaiser, A. Prabhu, C. Prescod-Weinstein and E. I. Sfakianakis, *Preheating after multifield inflation with nonminimal couplings, III: Dynamical spacetime results*, *Phys. Rev. D* **97** (2018) 023528 [[1610.08916](#)].
- [63] R. Nguyen, J. van de Vis, E. I. Sfakianakis, J. T. Giblin and D. I. Kaiser, *Nonlinear Dynamics of Preheating after Multifield Inflation with Nonminimal Couplings*, *Phys. Rev. Lett.* **123** (2019) 171301 [[1905.12562](#)].
- [64] J. van de Vis, R. Nguyen, E. I. Sfakianakis, J. T. Giblin and D. I. Kaiser, *Time-Scales for Nonlinear Processes in Preheating after Multifield Inflation with Nonminimal Couplings*, [2005.00433](#).
- [65] D. Baumann, *Inflation*, in *Theoretical Advanced Study Institute in Elementary Particle Physics: Physics of the Large and the Small*, pp. 523–686, 2011, [0907.5424](#), DOI.
- [66] PLANCK collaboration, Y. Akrami et al., *Planck 2018 results. X. Constraints on inflation*, [1807.06211](#).
- [67] S. Dodelson and L. Hui, *A Horizon ratio bound for inflationary fluctuations*, *Phys. Rev. Lett.* **91** (2003) 131301 [[astro-ph/0305113](#)].
- [68] A. R. Liddle and S. M. Leach, *How long before the end of inflation were observable perturbations produced?*, *Phys. Rev. D* **68** (2003) 103503 [[astro-ph/0305263](#)].
- [69] E. H. Tanin and T. Tenkanen, *Gravitational wave constraints on the observable inflation*, [2004.10702](#).
- [70] SIMONS OBSERVATORY collaboration, P. Ade et al., *The Simons Observatory: Science goals and forecasts*, *JCAP* **02** (2019) 056 [[1808.07445](#)].
- [71] R. Fakir and W. Unruh, *Improvement on cosmological chaotic inflation through nonminimal coupling*, *Phys. Rev. D* **41** (1990) 1783.
- [72] R. Fakir, S. Habib and W. Unruh, *Cosmological density perturbations with modified gravity*, *Astrophys. J.* **394** (1992) 396.
- [73] D. I. Kaiser, *Primordial spectral indices from generalized Einstein theories*, *Phys. Rev. D* **52** (1995) 4295 [[astro-ph/9408044](#)].
- [74] E. Komatsu and T. Futamase, *Complete constraints on a nonminimally coupled chaotic inflationary scenario from the cosmic microwave background*, *Phys. Rev. D* **59** (1999) 064029 [[astro-ph/9901127](#)].
- [75] V. Faraoni, *A Crucial ingredient of inflation*, *Int. J. Theor. Phys.* **40** (2001) 2259 [[hep-th/0009053](#)].
- [76] S. Tsujikawa and B. Gumjudpai, *Density perturbations in generalized Einstein scenarios and constraints on nonminimal couplings from the Cosmic Microwave Background*, *Phys. Rev. D* **69** (2004) 123523 [[astro-ph/0402185](#)].
- [77] A. Linde, M. Noorbala and A. Westphal, *Observational consequences of chaotic inflation with nonminimal coupling to gravity*, *JCAP* **03** (2011) 013 [[1101.2652](#)].
- [78] A. Achúcarro, E. J. Copeland, O. Iarygina, G. A. Palma, D.-G. Wang and Y. Welling, *Shift-Symmetric Orbital Inflation: single field or multi-field?*, [1901.03657](#).
- [79] A. Achúcarro, G. A. Palma, D.-G. Wang and Y. Welling, *Origin of ultra-light fields during inflation and their suppressed non-Gaussianity*, [1908.06956](#).
- [80] A. Achúcarro and Y. Welling, *Orbital Inflation: inflating along an angular isometry of field space*, [1907.02020](#).
- [81] X. Chen and M. H. Namjoo, *Standard Clock in Primordial Density Perturbations and Cosmic Microwave Background*, *Phys. Lett. B* **739** (2014) 285 [[1404.1536](#)].
- [82] X. Chen, M. H. Namjoo and Y. Wang, *Models of the Primordial Standard Clock*, *JCAP* **02** (2015) 027 [[1411.2349](#)].
- [83] X. Chen, M. H. Namjoo and Y. Wang, *Quantum Primordial Standard Clocks*, *JCAP* **02** (2016) 013 [[1509.03930](#)].
- [84] X. Chen, M. H. Namjoo and Y. Wang, *A Direct Probe of the Evolutionary History of the Primordial Universe*, *Sci. China Phys. Mech. Astron.* **59** (2016) 101021 [[1608.01299](#)].
- [85] G. Domènech and M. Kamionkowski, *Lensing anomaly and oscillations in the primordial power spectrum*, [1905.04323](#).
- [86] M. Braglia, D. K. Hazra, L. Sriramkumar and F. Finelli, *Generating primordial features at large scales in two field models of inflation*, [2004.00672](#).
- [87] M. M. Anber and L. Sorbo, *Naturally inflating on steep potentials through electromagnetic dissipation*, *Phys. Rev. D* **81** (2010) 043534 [[0908.4089](#)].
- [88] P. Adshead, J. T. Giblin, T. R. Scully and E. I.

- Sfakianakis, *Gauge-preheating and the end of axion inflation*, *JCAP* **12** (2015) 034 [[1502.06506](#)].
- [89] P. Adshead, J. T. Giblin, T. R. Scully and E. I. Sfakianakis, *Magnetogenesis from axion inflation*, *JCAP* **10** (2016) 039 [[1606.08474](#)].
- [90] J. Garcia-Bellido, M. Peloso and C. Unal, *Gravitational waves at interferometer scales and primordial black holes in axion inflation*, *JCAP* **12** (2016) 031 [[1610.03763](#)].
- [91] P. Adshead, J. T. Giblin, M. Pieroni and Z. J. Weiner, *Constraining axion inflation with gravitational waves from preheating*, *Phys. Rev. D* **101** (2020) 083534 [[1909.12842](#)].
- [92] P. Adshead, J. T. Giblin, M. Pieroni and Z. J. Weiner, *Constraining axion inflation with gravitational waves across 29 decades in frequency*, *Phys. Rev. Lett.* **124** (2020) 171301 [[1909.12843](#)].
- [93] J. Chluba et al., *Spectral Distortions of the CMB as a Probe of Inflation, Recombination, Structure Formation and Particle Physics: Astro2020 Science White Paper*, *Bull. Am. Astron. Soc.* **51** (2019) 184 [[1903.04218](#)].
- [94] A. S. Josan, A. M. Green and K. A. Malik, *Generalised constraints on the curvature perturbation from primordial black holes*, *Phys. Rev. D* **79** (2009) 103520 [[0903.3184](#)].
- [95] E. McDonough, H. Bazrafshan Moghaddam and R. H. Brandenberger, *Preheating and Entropy Perturbations in Axion Monodromy Inflation*, *JCAP* **05** (2016) 012 [[1601.07749](#)].
- [96] K. D. Lozanov and M. A. Amin, *GFiRe: a Gauge Field integrator for Reheating*, *JCAP* **04** (2020) 058 [[1911.06827](#)].